LETTER

doi:10.1038/nature23450

m^{6}A mRNA methylation controls T cell homeostasis by targeting the IL-7/STAT5/SOCS pathways

Hua-Bing Li[1]*§, Jiyu Tong[1,2]*, Shu Zhu[1]*, Pedro J. Batista[3], Erin E. Duffy[4,5], Jun Zhao[1,6], Will Bailis[1], Guangchao Cao[1,2], Lina Kroehling[1], Yuanyuan Chen[1,7], Geng Wang[1], James P. Broughton[3], Y. Grace Chen[3], Yuval Kluger[6], Matthew D. Simon[4,5], Howard Y. Chang[3], Zhinan Yin[2]§ & Richard A. Flavell[1,8]§

N^6-methyladenosine (m^{6}A) is the most common and abundant messenger RNA modification, modulated by 'writers', 'erasers' and 'readers' of this mark[1,2]. *In vitro* data have shown that m^{6}A influences all fundamental aspects of mRNA metabolism, mainly mRNA stability, to determine stem cell fates[3,4]. However, its *in vivo* physiological function in mammals and adult mammalian cells is still unknown. Here we show that the deletion of m^{6}A 'writer' protein METTL3 in mouse T cells disrupts T cell homeostasis and differentiation. In a lymphopaenic mouse adoptive transfer model, naive *Mettl3*-deficient T cells failed to undergo homeostatic expansion and remained in the naive state for up to 12 weeks, thereby preventing colitis. Consistent with these observations, the mRNAs of SOCS family genes encoding the STAT signalling inhibitory proteins SOCS1, SOCS3 and CISH were marked by m^{6}A, exhibited slower mRNA decay and showed increased mRNAs and levels of protein expression in *Mettl3*-deficient naive T cells. This increased SOCS family activity consequently inhibited IL-7-mediated STAT5 activation and T cell homeostatic proliferation and differentiation. We also found that m^{6}A has important roles for inducible degradation of *Socs* mRNAs in response to IL-7 signalling in order to reprogram naive T cells for proliferation and differentiation. Our study elucidates for the first time, to our knowledge, the *in vivo* biological role of m^{6}A modification in T-cell-mediated pathogenesis and reveals a novel mechanism of T cell homeostasis and signal-dependent induction of mRNA degradation.

T cell differentiation and proliferation represent an exceptionally simple and tractable model system with which to understand the general principles of cellular specification and gene regulation. αβ naive T cells can differentiate and proliferate into distinct functional T helper effector subset cells in response to defined cytokines *in vitro* and different micro-environmental signals *in vivo*[5,6]. As m^{6}A plays an essential role during the cell fate patterning of embryonic stem cells *in vitro*, we hypothesized that m^{6}A might be an important regulator of T helper differentiation. To study the *in vivo* functions of m^{6}A, we generated conditional knockout mice for the m^{6}A writer protein METTL3 (Extended Data Fig. 1a), as *Mettl3* knockout (*Mettl3*-KO) mice are embryonic lethal[3]. CD4$^+$ T cells from CD4-Cre conditional *Mettl3*$^{lox/lox}$ mice displayed absence of both METTL3 and its associated METTL14 proteins (Extended Data Fig. 1b). Concomitantly, the overall RNA m^{6}A methylation levels in knockout cells were decreased to roughly 28% of that in wild-type cells (Extended Data Fig. 1c). Characterization of mouse immune cell populations in the steady state revealed that T cell homeostasis was abnormal in spleen and lymph nodes, but not thymus, exhibited by the fact that naive T cell numbers from lymph nodes were increased (Extended Data Fig. 1d–g).

To characterize the possible defects of the *Mettl3*-KO naive T cells, we used the defined *in vitro* TCR-dependent T cell differentiation system and found that *Mettl3*-deficient naive T cells exhibited reduction of T_H1 and T_H17 cells, an increase in T_H2 cells, and no changes in T_{reg} cells relative to wild-type naive T cells (Extended Data Fig. 2a, b). We also saw no significant differences in proliferation and apoptosis between the wild-type and knockout naive T cells in these cultures (Extended Data Fig. 2c, d). Together, these findings suggest that m^{6}A modification has an important role during CD4$^+$ T cell differentiation, but not in T cell apoptosis and TCR-mediated proliferation.

Upon adoptive transfer into lymphopaenic mice, naive T cells normally undergo homeostatic expansion in response to the elevated IL-7 levels in such mice and differentiate into effector T cells, causing colitis[7]. To study how *Mettl3* regulates naive T cell homeostasis *in vivo*, we adoptively transferred CD4$^+$CD25$^-$CD45RB^{hi} naive T cells into *Rag2*$^{-/-}$ mice, and found that mice receiving knockout naive T cells

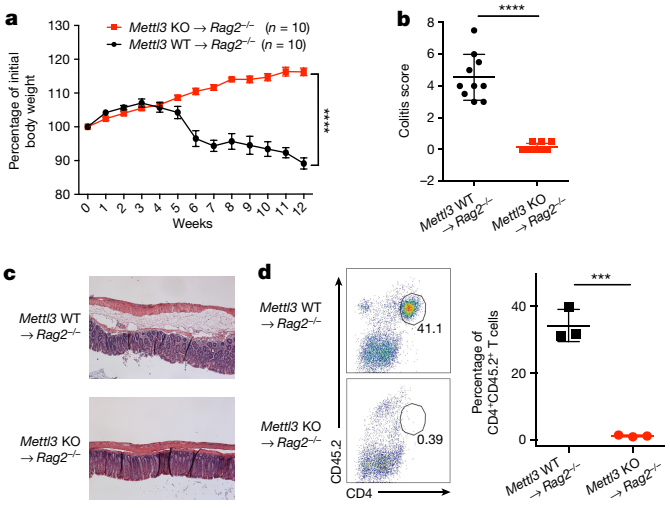

Figure 1 | *Mettl3*-KO naive T cells do not promote disease in CD45RB^{hi} adoptive transfer colitis mouse model. a, Body weight changes after naive T cell adoptive transfer into *Rag2*$^{-/-}$ host mice ($n = 10$), two-way ANOVA. **b**, **c**, Endoscopic colitis scores and representative pictures of haematoxylin and eosin staining of the colon from *Rag2*$^{-/-}$ receiving wild-type and knockout naive T cells 8 weeks after transfer ($n = 10$), unpaired *t*-test. **d**, FACS analysis of transferred T cells in colon tissues ($n = 3$), unpaired *t*-test. n = number of biological replicates. Repeated 3 times. ***$P < 0.001$, ****$P < 0.0001$.

[1]Department of Immunobiology, Yale University School of Medicine, New Haven, Connecticut 06520, USA. [2]The First Affiliated Hospital, Biomedical Translational Research Institute and Guangdong Province Key Laboratory of Molecular Immunology and Antibody Engineering, Jinan University, Guangzhou 510632, China. [3]Center for Dynamic Regulomes, Stanford University, Stanford, California 94305, USA. [4]Department of Molecular Biophysics & Biochemistry, Yale University, New Haven, Connecticut 06511, USA. [5]Chemical Biology Institute, Yale University, West Haven, Connecticut 06516, USA. [6]Department of Pathology, Yale University School of Medicine, New Haven, Connecticut 06520, USA. [7]Institute of Surgical Research, Daping Hospital, the Third Military Medical University, Chongqing 400038, China. [8]Howard Hughes Medical Institute, Chevy Chase, Maryland 20815-6789, USA.
*These authors contributed equally to this work.
§These authors jointly supervised this work.

(*Mettl3*$^{-/-}$ recipients) showed no signs of disease for up to 12 weeks after transfer. *Mettl3*$^{-/-}$ recipients continued to gain weight throughout the experiment, whereas control mice that received wild-type naive T cells (*Mettl3*$^{+/+}$ recipient) began losing weight in the fifth week after transfer (Fig. 1a). *Mettl3*$^{-/-}$ recipients exhibited no colitis upon endoscopy, displayed normal colon length, and were found to have reduced spleen and lymph node sizes compared to wild-type control mice at the eighth week after transfer (Fig. 1b, Extended Data Fig. 3a, b). When analysed by FACS, *Mettl3*$^{-/-}$ CD45.2 CD4^{+} donor T cells were nearly undetectable in recipient colons (Fig. 1d), as well as in the spleen, but instead remained in peripheral and mesenteric lymph nodes, whereas wild-type donor T cells were found in large numbers in all lymphoid organs of the recipients (Extended Data Fig. 3c, d). Haematoxylin and eosin staining and analysis of colons also confirmed that the *Mettl3*-KO T cells caused no T cell infiltration and inflammation, whereas wild-type T cells caused severe colonic inflammation and disrupted colon structure (Fig. 1c). Remarkably, FACS analysis further revealed that the vast majority of transferred *Mettl3*$^{-/-}$ T cells recovered from the peripheral lymph nodes still displayed their original naive T cell marker CD45RB^{+} as long as 12 weeks after transfer into *Rag2*$^{-/-}$ mice, whereas the transferred wild-type cells differentiated into the effector/memory T cells (CD45RB^{lo}) that mediated the pathology in this model (Fig. 2a).

We next sought to investigate whether *Mettl3*$^{-/-}$ naive T cells were capable of proliferation and could demonstrate normal survival after transfer into *Rag2*$^{-/-}$ mice[8]. Using CellTrace labelling of the transferred naive T cells, proliferation of wild-type cells was observable beginning from week 2, whereas *Mettl3*-KO T cells retained a naive phonotype and proliferated slowly. Four weeks after transfer, over 90% of wild-type cells had differentiated into effector/memory cells, while most of the *Mettl3*-KO T cells remained naive and failed to display increased proliferation (Fig. 2b, c). Despite starting with a similar number of cells, wild-type cells proliferated over 50 times more than *Mettl3*-KO cells by the second week, and over 400 times more by week four (Fig. 2d). No differences in apoptosis were observed between *Mettl3*-KO and wild-type T cells (Extended Data Fig. 3e), suggesting the differences in cell number were not due to defects in cell viability.

To establish that m^{6}A directly controls T cell homeostatic expansion, we re-introduced the wild-type *Mettl3* gene or m^{6}A catalytic-mutant *Mettl3* gene back into *Mettl3*-KO naive T cells, and showed that the wild-type *Mettl3* gene, but not m^{6}A catalytic-mutant *Mettl3*, could largely rescue the differentiation defects of *Mettl3*-KO naive T cells *in vivo* (Extended Data Fig. 3f, g). Furthermore, we also generated an additional CD4-Cre conditional mouse line for *Mettl14*, an essential m^{6}A catalytic partner for *Mettl3* in the same m^{6}A 'writer' complex. *Mettl14*-KO mice showed an identical phenotype to *Mettl3*-KO mice. Specifically, 4 weeks after transfer into *Rag2*$^{-/-}$ mice, *Mettl14*-KO naive T cells remained in the naive state (Fig. 2e), the mice displayed smaller lymphoid organs, and the cells expanded less than transferred wild-type naive T cells (Extended Data Fig. 4a-d). Taken together, our data suggest that m^{6}A RNA modification is required not only for T helper cell differentiation and proliferation *in vivo*, but also for T cells to properly exit the naive 'progenitor' state.

Peripheral T cell pools are maintained by complex mechanisms, and naive T cell homeostasis and survival is mainly sustained by the IL-7/STAT5 and self-peptide-MHC/TCR signalling axes[9]. It is well established that the elevated levels of IL-7 in lymphopaenic mice induce extensive homeostatic proliferation and differentiation of naive T cells after adoptive transfer[10]. We hypothesized that the IL-7 receptor and its downstream molecular pathway were compromised in *Mettl3*-KO cells. Consistently, we observed markedly decreased JAK1 and STAT5 phosphorylation levels in knockout naive T cells upon IL-7 stimulation (Fig. 3a). Moreover, basal ERK and AKT, but not NFκB, phosphorylation was found to be elevated in knockout naive T cells, with TCR stimulation only minimally enhancing ERK and AKT signalling. These findings are consistent with the observation that *Mettl3*-KO naive T cells proliferate normally *ex vivo* after TCR stimulation, indicating that the limited proliferation found after adoptive transfer to lymphopaenic mice was driven by defects in STAT5 phosphorylation, whereas their long-term survival in these recipients was maintained by elevated basal ERK and AKT signalling. We conclude that m^{6}A controls the balance of the two essential signalling pathways to control the T cell homeostasis, IL-7-mediated JAK–STAT signalling and TCR-mediated ERK/AKT signalling, thus uncoupling T cell proliferation from cell survival.

To explore further the molecular mechanism underlying the IL-7 signalling pathway defects, we performed RNA sequencing (RNA-seq) analysis on the naive T cells isolated from *Mettl3*-KO mice and littermate control wild-type mice. Consistent with our biochemical observations, the JAK–STAT and TCR signalling pathways were among the top upregulated KEGG pathways (Extended Data Fig. 5a, b, Supplementary Table 3). Notably, three Suppressor of cytokine signalling (SOCS) family genes (*Socs1*, *Socs3* and *Cish*) were among the most significantly upregulated genes. RNA-seq results were validated by qPCR and western blot,

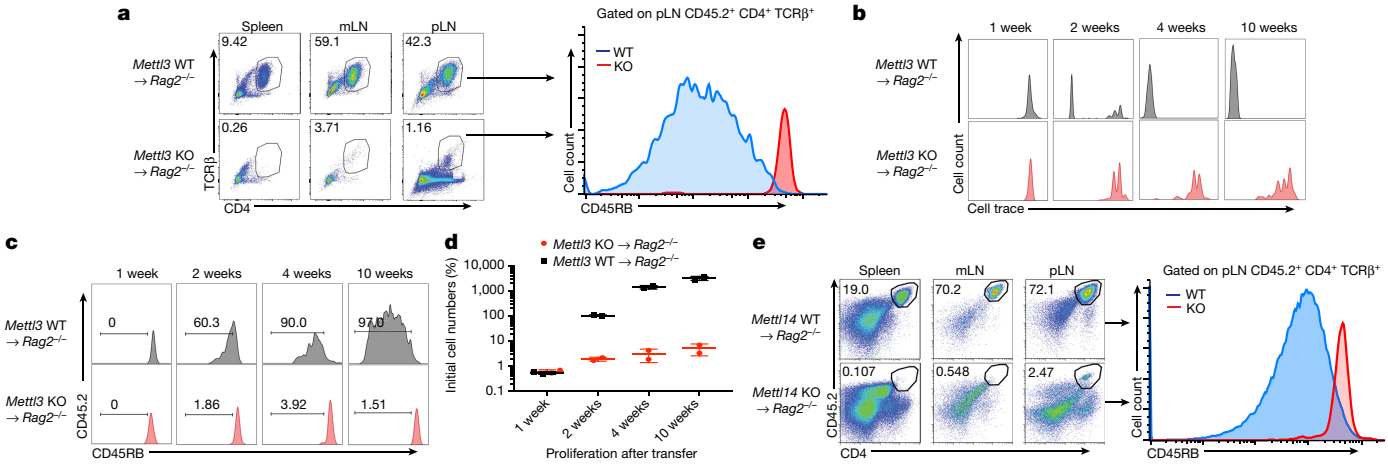

Figure 2 | Mettl3-KO naive T cells are locked in the naive state and proliferate much more slowly than wild-type cells after transfer into *Rag2*$^{-/-}$ mice. a, Most of the *Mettl3*-KO donor cells are retained in lymph nodes (LN) and are locked in naive states 12 weeks after transfer. **b**, The wild-type donor naive T cells start to differentiate from the second week after transfer (CD45RB^{lo}), whereas the *Mettl3*-KO donor naive T cells always stay in naive states (CD45RB^{hi}). **c**, **d**, The wild-type donor naive T cells are driven to proliferate rapidly from the second week, whereas the *Mettl3*-KO T cells proliferate slowly, with the total number of cells recovered from pLN shown in **d**. **e**, *Mettl14*-KO donor naive T cells recapitulate the phenotype of *Mettl3*-KO donor cells. At least six animals in each group were analysed, each experiment was repeated twice, and representative images are shown.

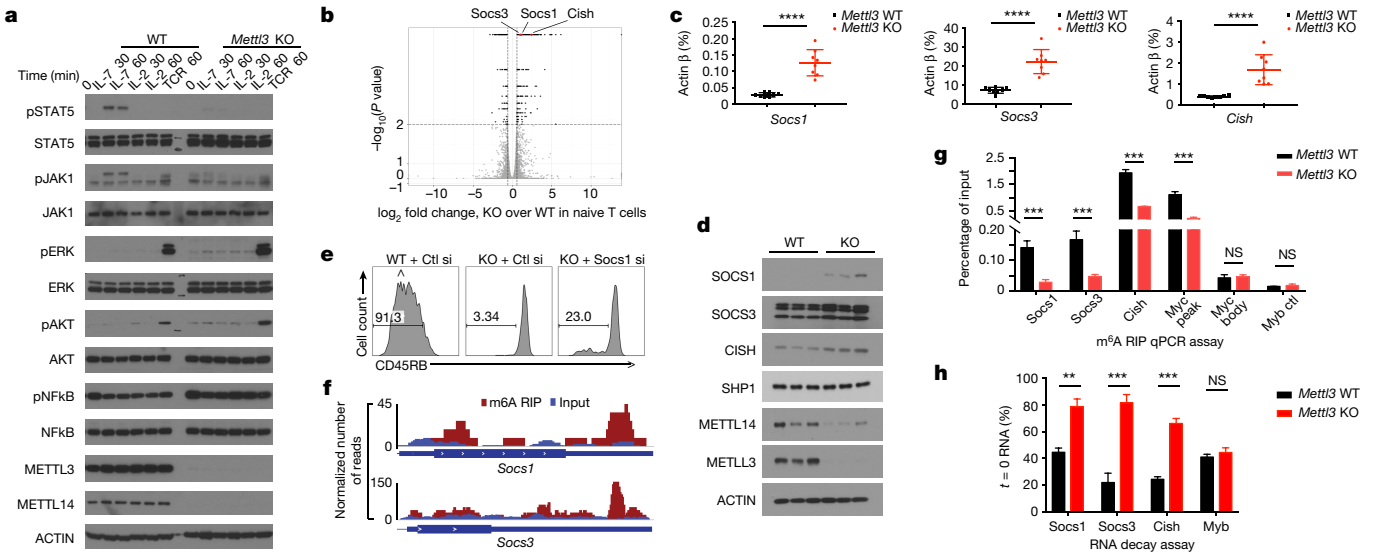

Figure 3 | Overexpressed m^{6}A target genes *Socs1*, *Socs3* and *Cish* in *Mettl3*-KO naive T cells suppress IL-7–STAT5 signalling pathway. **a**, Phosphorylation of STAT5 and JAK1 is diminished upon IL-7 stimulation *in vitro*, and basal levels of ERK and AKT phosphorylation are enhanced in knockout naive T cells. **b**, RNA-seq shows that *Socs1*, *Socs3* and *Cish* are among the most significantly upregulated genes in *Mettl3*-KO over wild-type naive T cells. **c**, **d**, RT–qPCR and western blots validate that *Socs1, Socs3* and *Cish* mRNA is overexpressed in *Mettl3*-KO versus wild-type naive T cells, unpaired *t*-test. **e**, *Socs1* siRNA knockdown in *Mettl3*-KO naive T cells partially rescues the differentiation defects 4 weeks after transfer into *Rag2*$^{-/-}$ mice. **f**, m^{6}A peaks are enriched in the 3′-UTRs of *Scos1* and *Socs3* genes from m^{6}A RIP-seq data with wild-type CD4$^+$ T cells. **g**, *Socs1*, *Socs3* and *Cish* are m^{6}A modified, and the marker is lost in *Mettl3*-KO naive T cells, two-way ANOVA. **h**, RNA degradation assay shows that *Socs1*, *Socs3* and *Cish* mRNAs degrade slower in *Mettl3*-KO naive T cells than in wild-type cells two hours after actinomycin-D treatment. The residual RNAs were normalized to $t = 0$. Three independent experiments were performed for all of the blots and qPCR assays. $^{**}P < 0.01$, $^{***}P < 0.001$, $^{****}P < 0.0001$, NS, not significant.

confirming that *Socs1*, *Socs3* and *Cish* were overexpressed and SOCS1 in particular showed even higher relative expression in *Mettl3*-KO naive T cells (Fig. 3c, d), whereas other important genes in IL-7 signalling pathways did not change (Extended Data Fig. 5c). SOCS proteins are the key physiological inhibitors of JAK–STAT signalling pathways and have important roles in T cell proliferation and differentiation[11,12]. In particular, SOCS1 is a well-known negative regulator of IL-7 signalling, and SOCS3 and CISH also inhibit STAT5 phosphorylation and T cell proliferation, while promoting ERK activity by binding to RasGAP[13–17]. Consistently, siRNA-mediated *Socs1* knockdown partially rescued the *in vivo* differentiation defects of *Mettl3*-KO naive T cells 4 weeks after adoptive transfer into *Rag2*$^{-/-}$ mice (Fig. 3e, Extended Data Fig. 5d). Altogether, overexpression of SOCS1, SOCS3 and CISH in *Mettl3*-KO cells probably synergistically suppresses IL-7/STAT5 signalling, and enhances ERK and AKT signalling, to inhibit naive T cell proliferation and differentiation but maintain its survival.

RNA m^{6}A methylation is understood to affect RNA stability, with *Mettl3* deletion resulting in loss of the m^{6}A marker and in turn slower RNA decay of m^{6}A targets[2–4,18]. To assess whether loss of *Mettl3* resulted in decreased m^{6}A methylation of SOCS family member mRNA, we performed genome-wide m^{6}A methylation profiling using m^{6}A-RIP-seq with wild-type CD4$^+$ T cells, and found that *Socs1* and *Socs3* mRNA 3′UTRs have highly enriched and specific m^{6}A peaks (Fig. 3f), which is consistent with published mouse embryonic stem cell (ES cell) and mouse dendritic cell m^{6}A-seq data sets[4,19] (Extended Data Fig. 5e). We confirmed by m^{6}A RNA-immunoprecipitation (RNA-IP) qPCR that *Socs1*, *Socs3* and *Cish* mRNAs were m^{6}A targets, and that m^{6}A was lost in *Mettl3*-KO naive T cells (Fig. 3g). Next, we performed RNA decay assays and found that *Socs1*, *Socs3* and *Cish* mRNA levels were all increased in *Mettl3*$^{-/-}$ cells in comparison to wild-type cells 2 h after actinomycin-D treatment (Fig. 3h). m^{6}A has also been reported to affect RNA splicing and translation[2–4,18]. To address these possibilities, we first performed genome-wide ribosome profiling, and found that ribosome occupancy and the calculated translation efficiency were not affected for all the related genes in *Mettl3*-KO cells versus wild-type cells (see Methods and Extended Data Fig. 6a–d, Supplementary Table 4). Next, we analysed our deep RNA-seq data, and did not find any splicing differences between *Mettl3*-KO and wild-type cells, suggesting that the naive T cell homeostasis defect is mainly due to m^{6}A-mediated degradation, rather than splicing or translation. Taken together, these data show that loss of m^{6}A modification in *Mettl3*-KO naive T cells leads to increased *Socs1*, *Socs3* and *Cish* mRNA half-life and protein levels, thus suppressing the IL-7/STAT5 signalling pathway.

mRNA levels are tightly regulated by both transcription and degradation[20]. While the abundance of most transcripts is mainly controlled by transcription rate, it has been shown that the mRNA levels of a minority of genes (~17%) are significantly regulated by mRNA degradation rates, notably immediate-early inducible genes[21,22]. *Socs* genes are well-known immediate-early genes induced upon IL-7 stimulation[11,12], thus we hypothesized that m^{6}A specifically targets 'signal-dependent immediate-early genes' for degradation. Interestingly, we found that upregulated genes (including *Socs1* and *Socs3*) in *Mettl3*-KO naive T cells were significantly enriched in the degradation-controlled group of genes from LPS-stimulated dendritic cells[20,21] (chi square test, $P < 0.0001$, Extended Data Fig. 7a). In addition, using the RNA decay assay we found that the mRNAs of all three *Socs* genes were degraded faster upon IL-7 stimulation, as early as 10 min after IL-7 stimulation, compared to control treatment in wild-type cells, whereas the accelerated mRNA degradation upon IL-7 stimulation was abrogated in *Mettl3*-KO naive T cells (Extended Data Fig. 7b). To extend our observation genome-wide and estimate the rates of synthesis and degradation, we conducted a time-course s^{4}U-seq with IL-7 induction and found a cluster of 34 transcripts including *Cish*, *Socs1* and *Socs3* that were increased in *Mettl3*-KO relative to wild-type cells and show similar kinetics of induction[23] (Fig. 4a, b; see also Methods, Extended Data Fig. 8a–c, Supplementary Table 5). This analysis also confirmed that the estimated degradation rates were lower in *Mettl3*-KO cells for Socs transcripts after IL-7 induction (Fig. 4c, d). We conclude that m^{6}A targets a group of immediate-early inducible genes including *Socs1*, *Socs3* and *Cish* for rapid mRNA degradation upon IL-7 stimulation, allowing IL-7/JAKs signalling to activate the

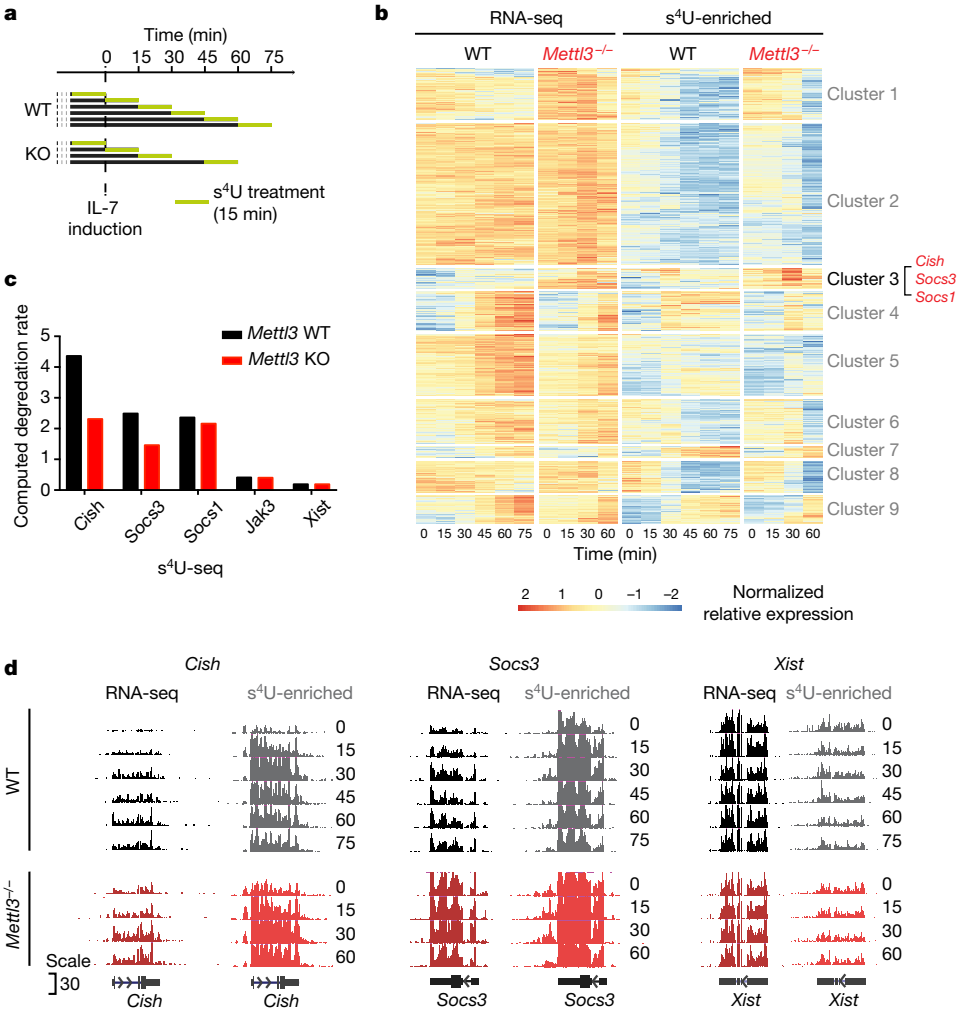

Figure 4 | m^{6}A specifically targets a group of immediate-early genes for degradation upon IL-7 stimulation. a, s^{4}U-seq experiment overview. **b**, Heatmap showing the results of clustering that normalizes transcript expression levels with significant changes after IL-7 induction and differences between wild-type and *Mettl3*$^{-/-}$. Cluster 3 contains 34 transcripts with similar expression profiles including *Cish*, *Socs3* and *Socs1*. **c**, Computed RNA degradation rates from s^{4}U-seq data. **d**, Read density for total RNA and s^{4}U-enriched RNA at the indicated genes for wild-type and *Mettl3*$^{-/-}$ samples after IL-7 stimulation.

downstream target STAT5, to initiate the re-programming of naive T cells for differentiation and proliferation.

T cell homeostasis is essential for maintaining the T cell pool size and forms the basis for adaptive immunity. Rather than the findings of m^{6}A functions in ES cells, here we have revealed a different strategy, whereby m^{6}A targets mRNAs encoding signalling proteins that control the 'gatekeeper' IL-7 signal in naive T cells, the progenitors of the adaptive immune system. Thus these targets expand the scope of m^{6}A biology and enable RNA modification to affect critical dynamic signalling systems and responses to external stimuli that maintain homeostasis. Specifically, using *Mettl3* and *Mettl14* conditional knockout mice, our current study demonstrates a novel mechanism whereby m^{6}A functions *in vivo* to control T cell homeostasis by inducible degradation of *Socs* gene family mRNA, and consequently relieves the block on IL-7 signalling and T cell proliferation (Extended Data Fig. 9). Our study implies that m^{6}A represents an evolutionarily conserved mechanism to specifically control the degradation rates of a group of immediate-early response genes in response to various environmental stimuli. Our study illustrates not only how this important epitranscriptomic marker has an essential role in development, but also that m^{6}A modifications act as a critical regulator of immune cell homeostasis and function, opening new avenues of investigation into the function of m^{6}A in human health and disease. As T cells regulate the entire adaptive immune response, this has broad implications. These findings further suggest that T cell-specific delivery of m^{6}A-modifying agents might be an effective treatment to alleviate various autoimmune diseases.

Online Content Methods, along with any additional Extended Data display items and Source Data, are available in the online version of the paper; references unique to these sections appear only in the online paper.

Received 3 October 2016; accepted 30 June 2017.
Published online 9 August 2017.

1. Cao, G., Li, H. B., Yin, Z. & Flavell, R. A. Recent advances in dynamic m^{6}A RNA modification. *Open Biol.* **6,** 160003 (2016).
2. Fu, Y., Dominissini, D., Rechavi, G. & He, C. Gene expression regulation mediated through reversible m^{6}A RNA methylation. *Nat. Rev. Genet.* **15,** 293–306 (2014).
3. Geula, S. *et al.* Stem cells. m^{6}A mRNA methylation facilitates resolution of naive pluripotency toward differentiation. *Science* **347,** 1002–1006 (2015).
4. Batista, P. J. *et al.* m^{6}A RNA modification controls cell fate transition in mammalian embryonic stem cells. *Cell Stem Cell* **15,** 707–719 (2014).
5. Collins, A. & Littman, D. R. Selection and lineage specification in the thymus: commitment 4-stalled. *Immunity* **23,** 4–5 (2005).
6. Esplugues, E. *et al.* Control of T$_H$17 cells occurs in the small intestine. *Nature* **475,** 514–518 (2011).
7. Ostanin, D. V. *et al.* T cell transfer model of chronic colitis: concepts, considerations, and tricks of the trade. *Am. J. Physiol. Gastrointest. Liver Physiol.* **296,** G135–G146 (2009).

8. Martin, C. E., Frimpong-Boateng, K., Spasova, D. S., Stone, J. C. & Surh, C. D. Homeostatic proliferation of mature T cells. *Methods Mol. Biol*. **979,** 81–106 (2013).
9. Takada, K. & Jameson, S. C. Naive T cell homeostasis: from awareness of space to a sense of place. *Nat. Rev. Immunol.* **9,** 823–832 (2009).
10. Sprent, J. & Surh, C. D. Normal T cell homeostasis: the conversion of naive cells into memory-phenotype cells. *Nat. Immunol.* **12,** 478–484 (2011).
11. Yoshimura, A., Naka, T. & Kubo, M. SOCS proteins, cytokine signalling and immune regulation. *Nat. Rev. Immunol.* **7,** 454–465 (2007).
12. Palmer, D. C. & Restifo, N. P. Suppressors of cytokine signaling (SOCS) in T cell differentiation, maturation, and function. *Trends Immunol.* **30,** 592–602 (2009).
13. Surh, C. D. & Sprent, J. Homeostasis of naive and memory T cells. *Immunity* **29,** 848–862 (2008).
14. Chong, M. M. *et al.* Suppressor of cytokine signaling-1 is a critical regulator of interleukin-7-dependent $CD8^+$ T cell differentiation. *Immunity* **18,** 475–487 (2003).
15. Cacalano, N. A., Sanden, D. & Johnston, J. A. Tyrosine-phosphorylated SOCS-3 inhibits STAT activation but binds to p120 RasGAP and activates Ras. *Nat. Cell Biol.* **3,** 460–465 (2001).
16. Matsumoto, A. *et al.* A role of suppressor of cytokine signaling 3 (SOCS3/CIS3/SSI3) in CD28-mediated interleukin 2 production. *J. Exp. Med.* **197,** 425–436 (2003).
17. Matsumoto, A. *et al.* Suppression of STAT5 functions in liver, mammary glands, and T cells in cytokine-inducible SH2-containing protein 1 transgenic mice. *Mol. Cell. Biol.* **19,** 6396–6407 (1999).
18. Yue, Y., Liu, J. & He, C. RNA N^6-methyladenosine methylation in post-transcriptional gene expression regulation. *Genes Dev.* **29,** 1343–1355 (2015).
19. Schwartz, S. *et al.* Perturbation of m^6A writers reveals two distinct classes of mRNA methylation at internal and 5′ sites. *Cell Reports* **8,** 284–296 (2014).
20. Tani, H. & Akimitsu, N. Genome-wide technology for determining RNA stability in mammalian cells: historical perspective and recent advantages based on modified nucleotide labeling. *RNA Biol.* **9,** 1233–1238 (2012).
21. Rabani, M. *et al.* Metabolic labeling of RNA uncovers principles of RNA production and degradation dynamics in mammalian cells. *Nat. Biotechnol.* **29,** 436–442 (2011).
22. Rabani, M. *et al.* High-resolution sequencing and modeling identifies distinct dynamic RNA regulatory strategies. *Cell* **159,** 1698–1710 (2014).
23. Duffy, E. E. *et al.* Tracking distinct RNA populations using efficient and reversible covalent chemistry. *Mol. Cell* **59,** 858–866 (2015).

Supplementary Information is available in the online version of the paper.

Acknowledgements We thank R. Flynn, R. Jackson, Y. Yang, M. Vesely, R. Paiva, N. Palm and all the other members of the Flavell laboratory for discussions and comments. We thank J. Alderman, C. Lieber, C. Hughes and J. Stein for technical support. H.-B.L. was supported by NIH T32 2T32DK007356. S.Z was supported by a fellowship from Helen Hay Whitney Foundation-Howard Hughes Medical Institute. This work was supported by the Howard Hughes Medical Institute (R.A.F.), NSF Major International Joint Research Program of China - 31420103901 (Z.Y. and R.A.F.) and '111' project (Z.Y.), R01-HG004361 (H.Y.C.), NIH New Innovator Award DP2 HD083992-01 (M.D.S.), and a Searle scholarship (M.D.S.).

Author Contributions H-B. L. conceived the project. H.-B. L., J. T., S. Z., P.B., E.E.D., W.B., G.C., Y. C., G.W., J.P.B. and Y.G.C. performed the experimental work. J.Z., L.K., M.D.S. and P.B. analysed the RNA-seq, ribo-profiling, s^4U-seq and m^6A-seq data and performed the statistical analysis. H.Y.C., M.D.S., Y.K., and Z.Y. provided key suggestions. H.-B. L. and R.A.F designed the study, analysed the data and wrote the manuscript. R.A.F. supervised the study.

Author Information Reprints and permissions information is available at www.nature.com/reprints. The authors declare no competing financial interests. Readers are welcome to comment on the online version of the paper. Publisher's note: Springer Nature remains neutral with regard to jurisdictional claims in published maps and institutional affiliations. Correspondence and requests for materials should be addressed to R.A.F. (richard.flavell@yale.edu), H.-B.L. (huabing.li@yale.edu) or Z.Y. (zhinan.yin@yale.edu).

Reviewer Information *Nature* thanks F. Fuks, J. H. Hanna and the other anonymous reviewer(s) for their contribution to the peer review of this work.

METHODS

Mice. *Mettl3* and *Mettl14* conditional knockout mice were both generated by inserting two lox sites into the first and the last introns using the CRISPR–Cas9-based genome-editing system as previously described[24] (Extended Data Fig. 1a). The gRNA and donor oligonucleotides used were as follows. For *Mettl3* left side lox: 5′-AGTGCTGCCATGTGAATGAAAGG-3′, and 5′-AG*T*A*GTTCTCTG GAAAATCCAGGATTATTTTGGCAAAACAGCAAGTGCTGCCATGTGAAT GAA**ATAACTTCGTATAATGTATGCTATACGAAGTTAT**AGGTGATCTAGAG CTAACGCTGGTCAGAGACCCTGCTTGAAGTGAAAGATGTGTGTGCTAGC G*A*T*G-3′; for *Mettl3* right side lox: 5′-ATACATTCTGGTAGTCTAGATGG-3′, and 5′-CC*C*C*C*CAAAAAACCCTTTATGGACAAAGACAGATGTCACTGAG TTGT ATACATTCTGGTAGTCTA**GAATAACTTCGTATAATGTATGCT ATACGAAGTTAT**TGGCTTAAGCTTTACCAGAATCTACAACATTCATTAGA ACCCAAAGGGCTGTTCTTAAAGCTC*T*A*A-3′. The gRNA and donor oligonucleotides used for *Mettl14* left side lox: 5′-CATAAAGTGGTTCAC ATGAAGGG-3′, and 5′-AA*T*G*AAGCTGAGTGCATCTCTGTGAGA GCAGGAGATACATGTAGTACATAAAGTGGTTCACATGAA**ATAACTTCGT ATAATGTATGCTATACGAAGTTAT**GGGCTTTGCTTTCTGTGTTACTGCTT CTGATGCCAACTTGTATTTCATTCACCATTGGCGACA*G*G*G-3′; for *Mettl14* right side lox: 5′-TACATAGATGAGGAACAATAAGG-3′, and 5′-AT*T*G*TGTATTAAAATATCTTTTCTAAGTGGTATTCTAACAACACAATA CATAGATGAGGAACAATA**ATAACTTCGTATAATGTATGCTATACGAAGTT AT**AGGATGATATGTAACAAAAGCTATAATCTAGAACGAGAAACAAGGTA TGTGCATATGGACCTT*T*T*T*A-3′. The donor oligonucleotides were synthesized by IDT with 5′- and 3′-ends modified by phosphorothioate bonds (denoted as *) to increase the oligonucleotide stability after delivered into mouse embryos. The pups born were genotyped and the PCR products were sequenced to validate intact integration of the lox sequences into the right genome loci.

We crossed floxed *Mettl3* or *Mettl14* mice with CD4-Cre mice to obtain conditional knockout mice. The CD4-Cre mice were purchased from the Jackson laboratory and have been fully backcrossed to C57BL/6 mice from the Charles River laboratories (over more than 10 generations).

Mettl3$^{fl/fl}$ without CD4-Cre, or only CD4-Cre mice had both been used as wild-type controls for *Mettl3*$^{fl/fl}$; CD4-Cre mice, and we found there were no signs of differences using either one regarding our observed phenotypes. Thereafter, we only used *Mettl3*$^{fl/fl}$ as wild-type controls for *Mettl3*$^{fl/fl}$; CD4-Cre knockout mice for most of the experiments reported here. All of the knockout and wild-type mice were littermates and co-housed for any experiments described. All the mice were bred and maintained under specific-pathogen-free conditions at the animal facility of Yale University School of Medicine. Animal procedures were approved by the Institutional Animal Care and Use Committee of Yale University. Both female and male mice were used in experiments. Wherever possible, preliminary experiments were performed to determine requirements for sample size, taking into account resources available and ethical, reductionist animal use. Exclusion criteria such as inadequate staining or low cell yield due to technical problems were pre-determined. Animals were assigned randomly to experimental groups. Each cage contained animals of all the different experimental groups.

Reagents and antibodies. The detailed information on all reagents and antibodies used in this study are listed in Supplementary Table 1.

CD45RB^{hi} adoptive transfer colitis, endoscopic and histologic analysis. We performed the experiment as described[7,25]. Briefly, pure CD4$^+$CD25$^-$CD45RB^{hi} naive T cells were sorted from wild-type and *Mettl3*-KO or *Mettl14*-KO mice by FACS, washed twice with PBS, counted, and intravenously injected 0.5 million cells into each *Rag2*$^{-/-}$ recipient mice. The recipient mice were monitored and weighted each week.

At week 7, colon colitis was visualized using Coloview system (Karl Storz). Briefly, colitis score was evaluated considering the consistence of stools, granularity of the mucosal surface, translucency of the colon, fibrin deposit and vascularization of the mucosa (0–3 points for each parameter). Haematoxilin and eosin staining was performed on paraffin sections of colon previously fixed in Bouin's fixative solution.

Cell proliferation and apoptosis assay. To trace T cell homeostatic proliferation *in vivo*, we labelled the FACS-purified CD4$^+$CD25$^-$CD45RB^{hi} naive cells with CellTrace (ThermoFisher Scientific, C34557) before intravenous injections[8]. We then intravenously injected 0.5 million cells into each *Rag2*$^{-/-}$ recipient mouse. We analysed the mice at 1 week, 2 weeks, 4 weeks and 10 weeks after injection by FACS using the naive T cell marker CD45RB for differentiation, and CellTrace violet for proliferation.

For apoptosis assay, we stained the *in vitro* cultured cells or cells from mice with annexin V and 7-AAD and analysed by FACS, in which double-negative cells are viable cells, whereas annexin V$^+$ or double-positive cells are apoptotic cells.

T cell *ex vivo* differentiation. We FACS sorted CD4$^+$C62L$^+$CD44^{lo} cells with FACSAria II Cell Sorter (BD Biosciences) and activated them with plate-bound monoclonal antibodies to CD3 (10 μg ml^{-1}, 145-2C11) and CD28 (1–2 μg ml^{-1}, PV-1) in the presence of mouse recombinant cytokines and blocking antibodies. Specifically, T_H1 direction with IL-12 (10 ng ml^{-1}) and antibody to IL-4 (11B11, 10 μg ml^{-1}); T_H2 direction with IL-4 (10 ng ml^{-1}) and antibody to IFN-γ (XMG1.2, 10 μg ml^{-1}); T_H17 with IL-6 (20 ng ml^{-1}), IL-23 (20 ng ml^{-1}), and antibodies to IFN-γ (XMG1.2, 10 μg ml^{-1}) and IL-4 (11B11, 10 μg ml^{-1}); iT_{reg} with TGF-β (2 ng ml^{-1}), IL-2 (50 U ml^{-1}), IL-23 (20 ng ml^{-1}), and antibodies to IFN-γ (XMG1.2, 10 μg ml^{-1}) and IL-4 (11B11, 10 μg ml^{-1}). All cytokines were purchased from R&D. Click's (Irvine Scientific) or RPMI (SIGMA-ALDRICH) (when indicated) media were supplemented with 10% FBS, L-glutamine (2 mM), penicillin (100 U ml^{-1}) and β-mercaptoethanol (40 nM). After 4 days of culture, the cells were analysed by FACS.

Signalling assay. Naive T cells were isolated by FACS, counted, and 1 million cells in cell culture media were plated on each well of 48-well plate. 10 μg of IL-7 or IL-2, or 0.2 μl of CD3/CD28 beads (ThermoFisher Scientific, 11452D) were added into the media, mixed and incubated at 37 °C. Cells were collected before adding cytokines or antibody beads ($t = 0$), or 30 min ($t = 30$) or 60 min ($t = 60$) after adding the cytokines or antibody beads. The cells were lysed on ice for 30 min in RIPA buffer (ThermoFisher Scientific, 89901) with protease inhibitor cocktails (ThermoFisher Scientific, 78437) and phosphatase inhibitor cocktails (ThermoFisher Scientific, 78428). The supernatants were then used for western blot.

RNA-seq. We isolated CD4$^+$ cells using StemCell mouse CD4$^+$ Kit (StemCell Technologies, catalogue 19852) from spleen and lymph nodes. Then pure CD4$^+$CD25$^-$CD45RB^{hi} naive T cells were isolated by FACS sorting. We used two pairs of wild-type and knockout mice for the experiment. Total RNAs were isolated with Direct-zol RNA MicroPrep kits (Zymo Research, R2062). Yale Center for Genome Analysis (YCGA) processed the total RNA by Ribo-Zero rRNA removal kit, constructed the libraries, and subject them to standard illumine HiSeq2000 sequencing, and obtained >40 million reads for each sample.

Raw RNA-sequencing reads were aligned to the mouse genome (mm10, GRCm38) with Tophat[26]. Gene expression levels were measured by Cufflinks and differential analysis was performed with Cuffdiff[27]. Genes were considered significantly differentially expressed if showing ≥1.5 fold change and <0.01 *P* value. Gene set analysis was performed and enriched KEGG pathways were obtained through online bioinformatics tools[28]. Volcano plot and pathway plot were generated with R package 'ggplot2'[29]. We used CuffDiff and rMATS to analyse possible splicing difference events, and did not find any significant difference between *Mettl3*-KO and wild-type samples[30].

RT–qPCR. Total RNA was isolated from naive T cells as described in the 'RNA-seq' section, then reverse transcribed using High-Capacity cDNA Reverse Transcription Kit (ThermoFisher Scientific, 4368814). Primers used for qPCR are included in Supplementary Table 2. All qPCRs were run on Bio-Rad CFX96 real-time system using iTaq Universal SYBR Green Supermix (Bio-Rad, #1725124). Actin-β was used as internal control to normalize the data across different samples.

RNA degradation assay. Naive T cells purified by FACS sorting were plated on 96-well plates with 0.5-million cells per well. Actinomycin-D (Sigma-Aldrich, A1410) was added to a final concentration of 5 μM, and cells were collected before or 2 h after adding actinomycin-D. Then the cells were processed as described in 'RT–qPCR', except that the data were normalized to the $t = 0$ time point.

For signalling-dependent degradation assay, we first treated the naive T cells with actinomycin-D for 1 h to fully inhibit transcription, then added IL-7 (10 μg ml^{-1}) or PBS as control into each well. Cells were lysed with Trizol LS at 0, 10 min, 20 min, 30 min, or 45 min after IL-7 addition.

HPLC quantification of m^{6}A levels. RNA was collected with RLT buffer (Qiagen) according to the manufacturer's instructions. Two rounds of poly(A) selection were performed using PolyA purist Mag kit (Ambion). 200 ng of poly(A)-selected RNA was digested with 1 unit of nuclease P1 in 50 mM NH_4OAc at 37 °C for 1 h, and sample was cleared on a 0.22-μm filter. HPLC was performed on an Agilent 1290 Infinity UPLC system coupled to the Agilent 6490 Triple Quad mass spectrometer with the iFunnel. For the LC, the A solvent was water with 0.1% formic acid and the B solvent was acetonitrile with 0.1% formic acid. The MS was in positive mode, scanning for the AMP and m^{6}A product ion of 136 and 150.1, respectively. Samples were run in duplicate, and m^{6}A/A ratios calculated.

m^{6}A RNA-IP-qPCR and m^{6}A RNA-IP-seq. Total RNA was isolated with TRIZOL, according to the manufacturer's instructions, and subjected to rRNA depletion with RiboMinus kit (Ambion). RNA was fragmented to ~100 nucleotide fragments with Ambion fragmentation reagent (40 s incubation at 94 °C). 200 ng of RNA was denatured and incubated with 20 μl of protein A beads, previously bound to 1 μg of anti-m^{6}A polyclonal antibody (Synaptic Systems) or rabbit IgG in 1× IPP

buffer (150 mM NaCl, 10 mM TRIS-HCL and 0.1% NP-40). RNA was incubated with the antibody for 3 h at 4 °C in 1× IPP buffer. Beads were washed twice with 1× IPP buffer, twice with low salt buffer (50 mM NaCl, 10 mM TRIS-HCL and 0.1% NP-40), twice with high salt buffer (500 mM NaCl, 10 mM TRIS-HCL and 0.1% NP-40) and once with 1× IPP buffer. RNA was eluted from the beads with 50 μl of RLT buffer, and purified with Qiagen RNeasy columns. RNA was eluted in 100 μl of RNase free water.

m^{6}A enrichment was analysed on a LightCycler 480 by RT–qPCR with One-Step RT–PCR Master Mix SYBR Green (Stratagene). The PCR was carried out using a standard protocol with melting curve. The amount of target was calculated using the formula: amount of target $= 2^{-\Delta\Delta C_t}$ (ref. 31). *Myc peak* was positive control, *Myc body* and *Myb* were negative controls for m^{6}A RIP–qPCR. Two tailed *t*-test for unequal, unpaired data sets with heteroscedastic variation was used to compare samples.

For m^{6}A RNA-IP-seq, we started with ~200–300 μg of total RNA from CD4$^+$ T cells isolated from wild-type mice using StemCell CD4$^+$ T cell kits. Using the same protocol with scale-up reagents, the eluted IP-RNA was concentrated by ethanol precipitation, and resolved in 10 μl DEPC water. 10 ng RNA from input and enriched IP-RNA samples were used for library preparation with the SMARTer Stranded Total RNA-seq Kit Pico Input Mammalian (Clontech) according to the manufacturer's instructions. Input and enriched samples were multiplexed with Illumia bar codes and sequenced using paired-end 2 × 75-nt cycles on an Illumina HiSeq 2500 instrument. To process m^{6}A-seq data, reads were aligned using Tophat2. Macs was then used for peak calling following the protocol in ref. 32. Samples were normalized to get pileup per million reads in each sample, using the number of reads which were left after filtering redundant tags from MACS[33]. Peaks were then visualized using IGV[34].

siRNA knockdown. *Socs1* siRNA and non-targeting control siRNA were purchased from GE-Dharmacon (E-043120-00-0005), and the experiments were carried out per the manufacturer's instructions. The naive T cells with siRNA transfection were incubated at 37 °C for 3 h, then were transferred into *Rag2*$^{-/-}$ recipient mice by intravenous injection (1 million cells per mouse). Four weeks after transfer, the cells from spleen, peripheral lymph nodes, and mesenteric lymph nodes were analysed by FACS. Representative FACS images show that the naive marker CD45RB peaks shift leftwards upon *Socs1* siRNA treatment.

***Mettl3*-KO rescue.** The wild-type and catalytic dead *Mettl3* genes were cloned into N103 plasmid in the Chang laboratory. To create a catalytic dead mutant *Mettl3*, we inserted the mutations D395A and W398A (DPPW catalytic motif of METTL3) based on published data, which show that these two residues are absolutely required for METTL3 activity[35–37]. *Mettl3*-KO naive T cells were isolated from *Mettl3*-KO mice with StemCell naive T cell purification kit, then electroporated by nucleofection by exactly following the Amaxa mouse T cell nucleofector kit manual (Lonza). 4 h after nucleofection at 37 °C, the cells were transferred into *Rag2*$^{-/-}$ receipt mice by intravenous injection (1 million cells per mouse). Four weeks after transfer, the cells from spleen, periphery lymph nodes, and mesenteric lymph nodes were analysed by FACS for cell numbers, and naive cell marker CD45RB. The CD4$^+$ T cells were isolated from lymph nodes using StemCell CD4$^+$ T cell kit, and total RNA was isolated from the CD4$^+$ T cells using Direct-zol RNA microprep columns (Zymo Research). RT-qPCR was performed using the isolated RNAs. Each group had at least five mice to ensure statistical significance.

Ribosome profiling. We performed the ribosome profiling by strictly following the manual for the Illumina TruSeq Ribo Profile (Mammalian) Kit. Briefly, 50 million naive T cells were isolated from wild-type and *Mettl3*-KO mice, and washed and treated with 0.1 mg ml^{-1} cycloheximide for 1 min. After lysis, one-tenth of the cell lysate was used to isolate RNA for preparing input RNA library, the remainder was used to prepare ribosome footprints by being first digested with 60U of 10 U μl^{-1} nuclease, then cleaned up by MicroSpin S-400 columns. The total RNAs and ribosome protected RNAs were then isolated with RNA Clean & Concentrator-25 kit (Zymo Research), and subjected to rRNA removal with Illumina Ribo-Zero Gold Kits. Polyacrylamide gel electrophoresis (PAGE) was used to purify the 28-nt and 30-nt long ribosome protected fragments, which were ligated 3′ adapters and prepared cDNA library. The cDNA library was PAGE gel purified again for the 70–80-nt fragments, circularized, and amplified by PCR for nine cycles, and the resulting libraries were cleaned up by AMPure XP beads, purified by PAGE purification for ~140–160 bp fragments, and subjected to Illumina Hi-seq for 75bp paired-end sequencing.

We used the tuxedo suite (https://www.ccb.jhu.edu/software/tophat/) to align the ribosome profiling reads and determine FPKM, fold change, and the associated *P* value. All genes which did not have enough reads aligned to determine FPKM were discarded, and the remaining genes were plotted. To calculate translation efficiency, HTseq was used to count the number of reads in each experiment. The normalized translation efficiency was calculated by taking the $\log_2$ of the quotient of the ribosome footprint read count divided by the mRNA-seq read count. The individual graphs were plotted using R package (https://bioconductor.org/packages/release/bioc/html/Sushi.html).

Enrichment of s4U-labelled RNA. Naive T cells were isolated from *Mettl3*-KO and wild-type mice with naive T cell purification kits (StemCell). The cells were counted and aliquoted at 4-million per 1 ml FACS buffer per Eppendorf tube. Each tube except $t = 0$ received 10 μg ml^{-1} IL-7 cytokine and was incubated at 37 °C. 15 min before being spun down and lysed with Trizol, the cells were labelled with 250 μM s^{4}U. The enrichment of s^{4}U-RNA was performed using MTS-biotin chemistry[23,38]. Briefly, cells were lysed in TRIzol, extracted with chloroform once and the nucleic acids precipitated with isopropanol. DNA was removed with DNase, the proteins removed with phenol:chloroform:isoamylalcohol extraction, and RNA isolated using isopropanol precipitation. Total RNA was sheared to ~200 bp by adding shearing buffer (150 mM Tris-HCl, pH 8.3, 225 mM KCl, 9 mM $MgCl_2$) and heating to 94 °C for 4 min, followed by quenching on ice with EDTA. Sheared RNA was purified using a modified protocol with the RNeasy Mini Kit (Qiagen). To biotinylate the s4U-RNA, 20 μg sheared RNA was incubated with 2 μg MTS-biotin in biotinylation buffer for 30 min. Excess biotin was removed via chloroform extraction using Phase-Lock Gel Tubes. RNA was precipitated with a 1:10 volume of 3 M NaOAc and an equal volume of isopropanol and centrifuged at 20,000*g* for 20 min. The pellet was washed with an equal volume of 75% ethanol. Purified RNA was dissolved in 50 μl RNase-free water. Biotinylated RNA was separated from non-labelled RNA using glycogen-blocked Dynabeads Streptavidin C1 Beads (Invitrogen). Beads (10 μl) were added to each sample and incubated for 15 min at room temperature, then washed three times with high salt wash buffer (100 μl each, 100 mM Tris-HCl (pH 7.4), 10 mM EDTA, 1 M NaCl, and 0.1% Tween-20). In order to improve the stringency of the washes, an additional three washes with buffer TE (10 mM Tris pH 7.4, 1 mM EDTA) at 55 °C were added to the protocol. s^{4}U-RNA was eluted from Dynabeads with 25 μl freshly prepared elution buffer (10 mM DTT, 100 mM NaCl, 10 mM Tris pH 7.4, 1 mM EDTA, 10 pg μl *Schizosaccharomyces pombe* total RNA (a gift from J. Berro)) and incubated for 15 min, followed by a second elution with an additional 25 μl elution buffer. Both elutions were pooled and purified by ethanol precipitation. 1% input (200 ng sheared RNA) was also saved from each sample before enrichment, and 500 pg *S. pombe* total RNA was added as a normalization spike-in.

s^{4}U-seq library preparation and sequencing. 10ng RNA from input and enriched RNA samples was used for library preparation with the SMARTer Stranded Total RNA-seq Kit Pico Input Mammalian (Clontech) according to the manufacturer's instructions. Input and enriched samples were multiplexed with Illumina bar codes and sequenced using single-end 1 × 75-nt cycles on an Illumina HiSeq instrument.

Mapping and quantification of s^{4}U-seq libraries. Sequencing reads were aligned using STAR (version 2.4.2a; Dobin 2013) to a joint index of the *M. musculus* and *S. pombe* genomes (mm10 and sp2) and transcriptomes (UCSC and Ensembl Fungi v22)[39,40]. Alignments and analysis were performed on the Yale High Performance Computing clusters. Following alignment, HTSeq-count (version 0.6.1p1) was used to quantify annotated *M. musculus* and *S. pombe* transcripts for total RNA (-t gene) and mRNA (-t exon)[41]. Tracks normalized using the *S. pombe* reads were uploaded to the UCSC genome browser. The scale was normalized using exogenous *S. pombe* RNA added before library preparation.

Transcript abundance, synthesis and degradation rates were estimated using the INSPEcT package in R[42]. Spearman correlation between samples were visualized using the corrplot package. Transcripts with significant time-dependent changes were determined and clustered using the maSigPro package in R and heatmaps were made using the pheatmap package[43].

Statistical analysis. The sample size chosen for our animal experiments in this study was estimated based on our prior experience of performing similar sets of experiments. No statistical methods were used to predetermine sample size. All animal results were included and no method of randomization was applied. The experimenters were not blinded to allocation during experiments and outcome assessment. We independently repeated the data at least once, and all attempts to reproduce the results were successful. For all the bar graphs, data are expressed as mean ± s.e.m. Statistical analyses were performed using GraphPad Prism 6. Differences were analysed by Student's *t*-test or two-way ANOVA test using GraphPad Prism 6. *P* values ≤ 0.05 were considered significant ($^*P < 0.05$; $^{**}P < 0.001$; $^{***}P < 0.0001$); *P* values >0.05; non-significant (NS). FlowJo (Treestar) was used to analyse all the flow cytometry data. The sample sizes (biological replicates), specific statistical tests used, and the main effects of our statistical analyses for each experiment were detailed in each figure legend.

Data availability. The data that support the findings of this study are available from the corresponding author upon reasonable request. RNA-seq, ribosome profiling, s4U-seq, and m^{6}A RIP-seq data sets have been deposited in Gene Expression Omnibus under the accession number GSE100048.

24. Henao-Mejia, J. *et al.* Generation of genetically modified mice using the CRISPR–Cas9 genome-editing system. *Cold Spring Harb. Protoc.* http://dx.doi.org/10.1101/pdb.prot090704 (2016).
25. Gagliani, N. *et al.* T_H17 cells transdifferentiate into regulatory T cells during resolution of inflammation. *Nature* **523,** 221–225 (2015).
26. Kim, D. *et al.* TopHat2: accurate alignment of transcriptomes in the presence of insertions, deletions and gene fusions. *Genome Biol.* **14,** R36 (2013).
27. Trapnell, C. *et al.* Transcript assembly and quantification by RNA-seq reveals unannotated transcripts and isoform switching during cell differentiation. *Nat. Biotechnol.* **28,** 511–515 (2010).
28. Wang, J., Duncan, D., Shi, Z. & Zhang, B. WEB-based GEne SeT AnaLysis Toolkit (WebGestalt): update 2013. *Nucleic Acids Res.* **41,** W77–W83 (2013).
29. Wickham, H. ggplot2: elegant graphics for data analysis. http://dx.doi.org/10.1007/978-0-387-98141-3 (2009).
30. Shen, S. *et al.* rMATS: robust and flexible detection of differential alternative splicing from replicate RNA-seq data. *Proc. Natl Acad. Sci. USA* **111,** E5593–E5601 (2014).
31. Livak, K. J. & Schmittgen, T. D. Analysis of relative gene expression data using real-time quantitative PCR and the $2\Delta\Delta C_t$ Method. *Methods* **25,** 402–408 (2001).
32. Dominissini, D., Moshitch-Moshkovitz, S., Salmon-Divon, M., Amariglio, N. & Rechavi, G. Transcriptome-wide mapping of N^6-methyladenosine by m^6A-seq based on immunocapturing and massively parallel sequencing. *Nat. Protocols* **8,** 176–189 (2013).
33. Zhang, Y. *et al.* Model-based analysis of ChIP-seq (MACS). *Genome Biol.* **9,** R137 (2008).
34. Robinson, J. T. *et al.* Integrative genomics viewer. *Nat. Biotechnol.* **29,** 24–26 (2011).
35. Śledź, P. & Jinek, M. Structural insights into the molecular mechanism of the m^6A writer complex. *eLife* **5,** e18434 (2016).
36. Clancy, M. J., Shambaugh, M. E., Timpte, C. S. & Bokar, J. A. Induction of sporulation in *Saccharomyces cerevisiae* leads to the formation of N^6-methyladenosine in mRNA: a potential mechanism for the activity of the *IME4* gene. *Nucleic Acids Res.* **30,** 4509–4518 (2002).
37. Wang, P., Doxtader, K. A. & Nam, Y. Structural basis for cooperative function of Mettl3 and Mettl14 methyltransferases. *Mol. Cell* **63,** 306–317 (2016).
38. Duffy, E. E. & Simon, M. D. Enriching s^4U-RNA using methane thiosulfonate (MTS) chemistry. *Curr. Protoc. Chem. Biol.* **8,** 234–250 (2016).
39. Rosenbloom, K. R. *et al.* The UCSC Genome Browser database: 2015 update. *Nucleic Acids Res.* **43,** D670–D681 (2015).
40. Kersey, P. J. *et al.* Ensembl Genomes: an integrative resource for genome-scale data from non-vertebrate species. *Nucleic Acids Res.* **40,** D91–D97 (2012).
41. Anders, S., Pyl, P. T. & Huber, W. HTSeq—a Python framework to work with high-throughput sequencing data. *Bioinformatics* **31,** 166–169 (2015).
42. de Pretis, S. *et al.* INSPEcT: a computational tool to infer mRNA synthesis, processing and degradation dynamics from RNA- and 4sU-seq time course experiments. *Bioinformatics* **31,** 2829–2835 (2015).
43. Nueda, M. J., Tarazona, S. & Conesa, A. Next maSigPro: updating maSigPro bioconductor package for RNA-seq time series. *Bioinformatics* **30,** 2598–2602 (2014).

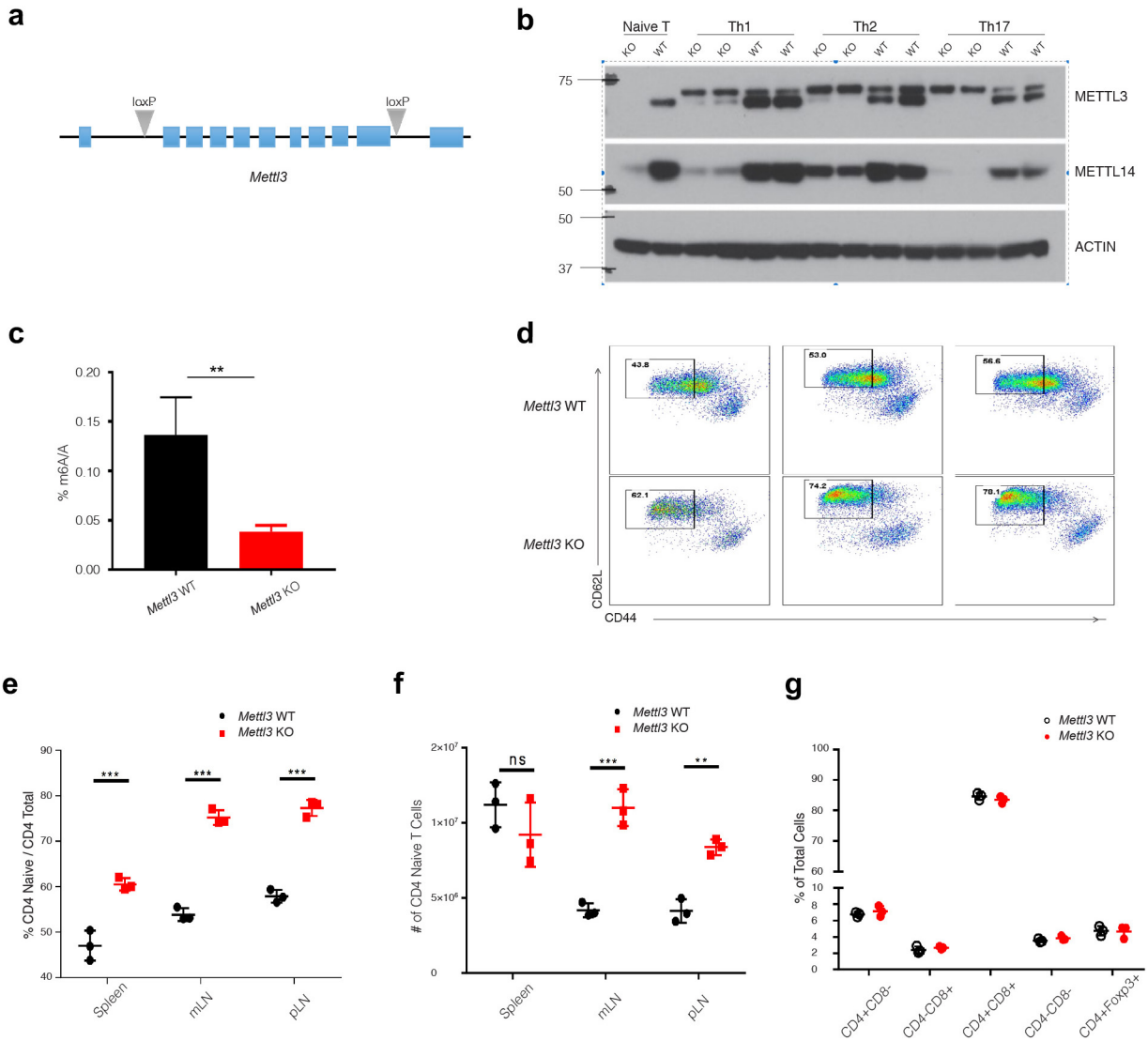

Extended Data Figure 1 | Abnormal T cell homeostasis in generated *Mettl3* CD4-Cre conditional knockout mice. a, The two lox sites were inserted into the first and last introns by CRISPR technology. **b**, Protein levels of METTL3 and its associated METTL14 were analysed by western blot in the naive T cells and in *in vitro* differentiated T_H1, T_H2 and T_H17 cells from *Mettl3*-KO and wild-type mice. **c**, Overall levels of RNA m^6A methylation in naive T cells from *Mettl3*-KO and wild-type mice ($n = 3$, $P = 0.0032$). **d**, Naive T cells increased in all lymphoid organs from *Mettl3*-KO mice compared to littermate control wild-type mice. Cells from spleen (SPL), mesenteric lymph node (mLN), and peripheral lymph node (pLN) were analysed by FACS by staining with CD4/CD44/CD62L. **e**, **f**, The percentage of $CD4^+CD44^{lo}CD62^+$ naive T cells increased in all three lymphoid organs in *Mettl3*-KO mice (**e**) and the total number of naive T cells in mLN and pLN also increased in knockout mice (**f**; $n = 3$). **g**, The cell population in the thymus did not change in *Mettl3*-KO ($n = 3$). n = number of biological replicates. Repeated three times and one set of data is shown. $^{**}P < 0.01$, $^{***}P < 0.001$.

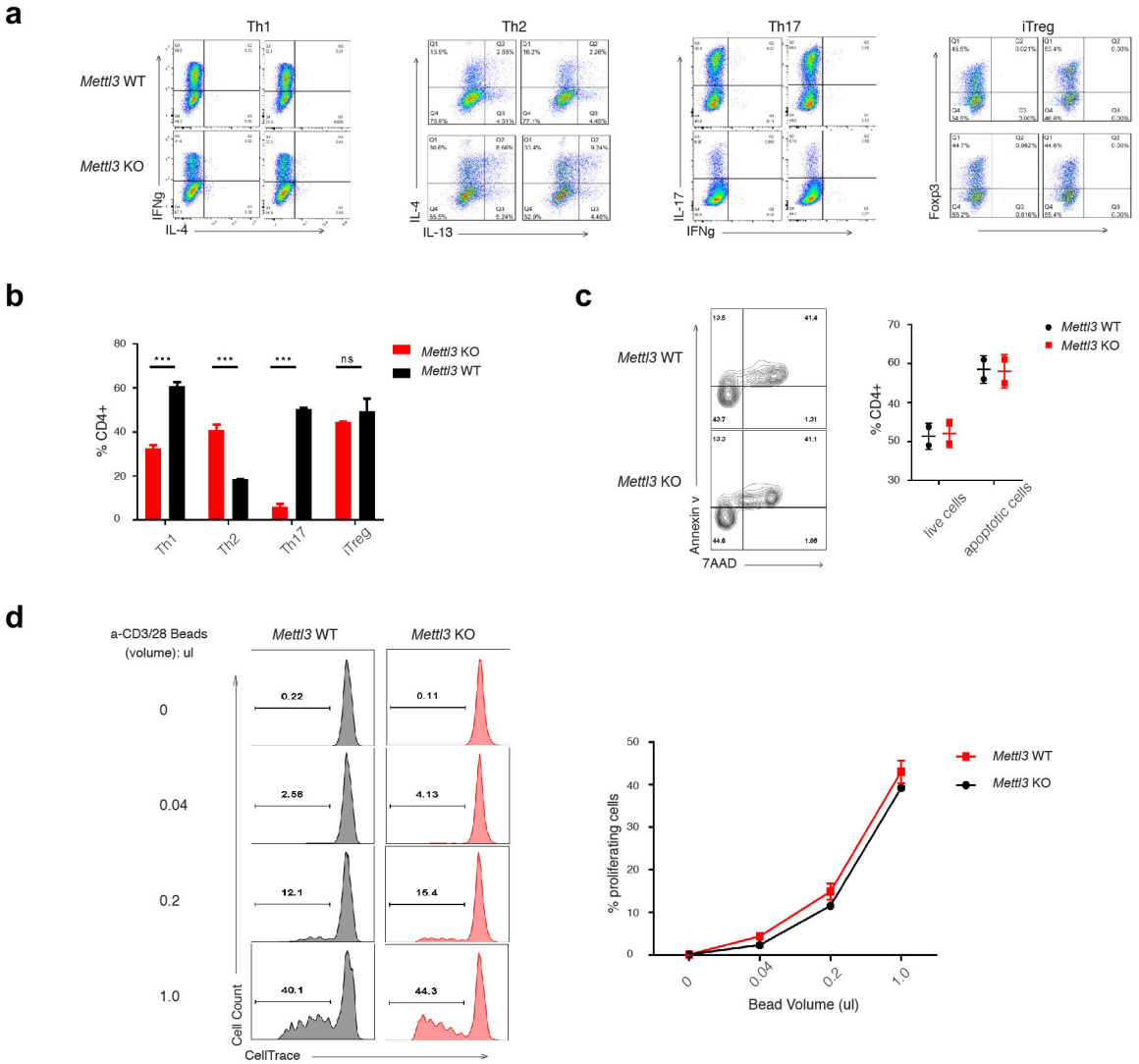

Extended Data Figure 2 | Naive T cells from *Mettl3*-KO mice differentiated into fewer T_H1 and T_H17 cells and more T_H2 cells *ex vivo* compared to wild-type naive T cells. a, Naive T cells isolated from *Mettl3* wild-type and knockout mice were differentiated into effector subsets under defined optimal conditions. **b**, The percentages of each T cell subtype over total $CD4^+$ T cells were analysed by FACS ($n = 3$). **c**, No apoptosis defects were found in *ex vivo* cultured cells from wild-type and *Mettl3*-KO naive T cells by FACS staining of annexin V and 7AAD. Double-negative stained cells are live cells, and the remaining are apoptotic cells. The percentage is listed in the right graph ($n = 2$). **d**, No proliferation differences were found in *ex vivo* cultured cells from wild-type and *Mettl3*-KO naive T cells. Naive T cells labelled with CellTrace were cultured *ex vivo* under different concentrations of anti-CD3/CD28 beads for 4 days. The percentages of proliferating cells are listed in the right graph ($n = 2$). n = number of biological replicates. Repeated three times and one set of data is shown. $^{***}P < 0.001$.

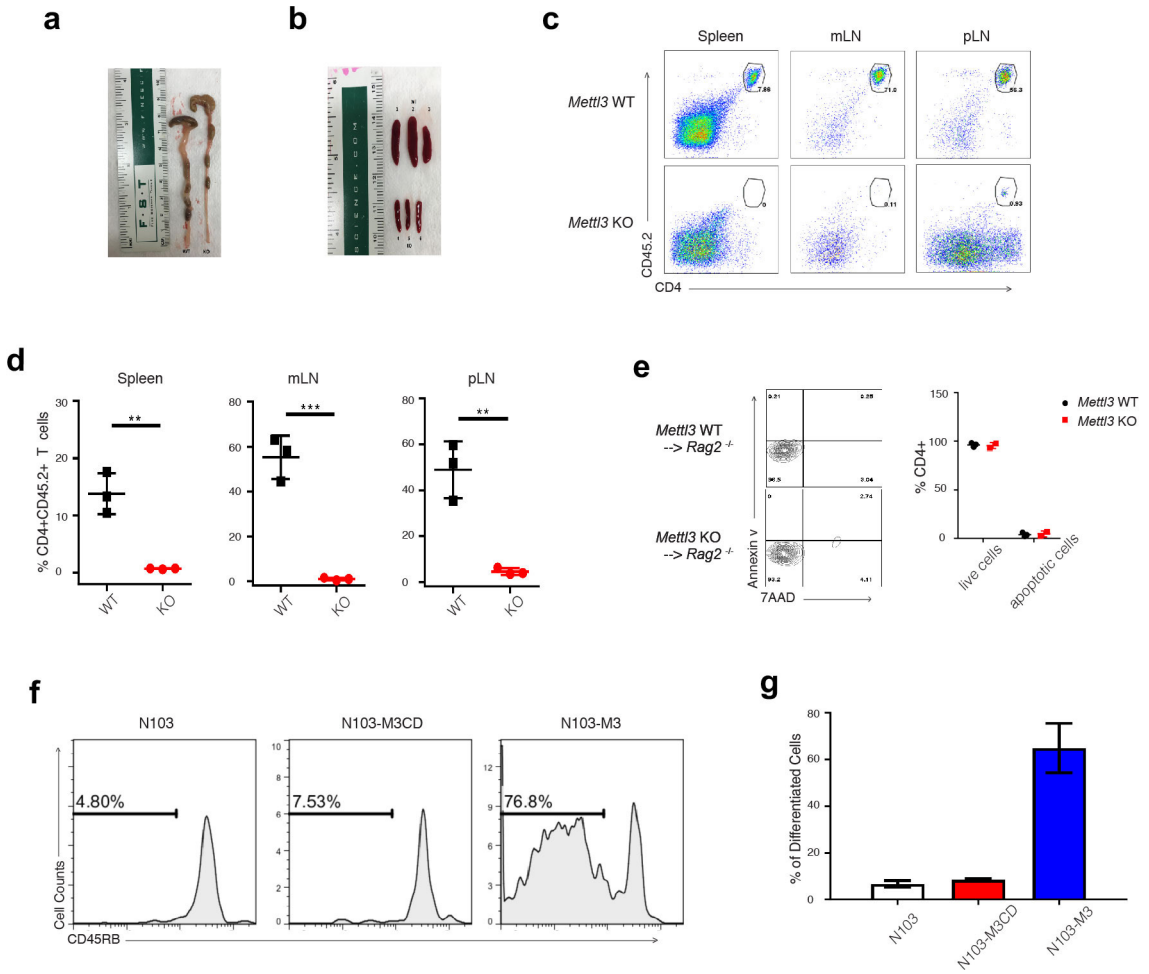

Extended Data Figure 3 | m^{6}A methylation function of *Mettl3* controls naive T cell homeostatic expansion. a, *Mettl3*$^{-/-}$ recipients had normal colon length, and *Mettl3*$^{+/+}$ recipients had shorter colon length. **b**, *Mettl3*$^{+/+}$ recipients had enlarged spleens indicative of normal homeostatic expansion, while *Mettl3*$^{-/-}$ recipients had very small spleens. **c**, All lymph organs had many fewer transferred knockout cells compared to wild-type cells analysed by FACS. **d**, The percentage of transferred *Mettl3*-KO and wild-type cells in *Rag2*$^{-/-}$ host mice ($n = 3$). **e**, No apoptosis defects were found in *in vivo* cells recovered from peripheral lymph nodes of *Mettl3* wild-type and knockout recipient mice by FACS staining of annexin V and 7AAD. Double-negative stained cells are live cells, and the remainder are apoptotic cells. The percentage is listed in the right graph ($n = 3$). **f**–**g**, Wild-type *Mettl3* constructs, but not m^{6}A catalytic dead *Mettl3* constructs, could rescue *Mettl3*-KO phenotypes *in vivo*. Empty construct (N103), catalytic dead *Mettl3* construct (N103-CD), and wild-type *Mettl3* construct (N103-M3) were electroporated into *Mettl3*-KO naive T cells, and then transferred into *Rag2*$^{-/-}$ mice. Four weeks after transfer, the cell number (proliferation) and CD45RB marker (differentiation) were analysed by FACS. Representative images are shown in **f**, and the numbers of cells are shown in **g** ($n = 3$). n = number of biological replicates. Repeated twice and one set of data is shown. $^{**}P < 0.01$, $^{***}P < 0.001$.

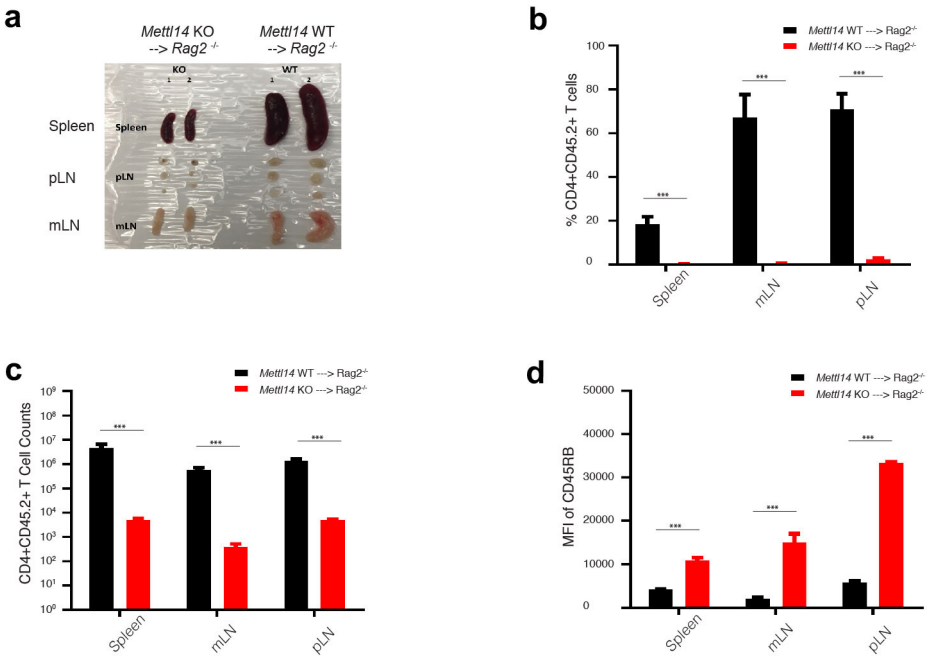

Extended Data Figure 4 | *Mettl14*-KO naive T cell adoptive transfer pheno-copies *Mettl3*-KO cells. a, *Mettl14*-KO recipient mice have smaller lymphoid organs, including spleen, peripheral lymph nodes, and mesenteric lymph nodes. **b**, **c**, The percentage and the number of transferred *Mettl14*-KO cells in $Rag2^{-/-}$ recipient mice were much lower than those of wild-type cells 4 weeks after transfer in all lymphoid organs (n=3). **d**, The MFI (median fluorescence intensity) of naive cell marker CD45RB is much higher in knockout than wild type, suggesting *Mettl14* naive T cells were locked in naive state, whereas wild-type naive T cells differentiated after 4 weeks in $Rag2^{-/-}$ mice ($n=3$). $n=$ number of biological replicates. Repeated twice and one set of data is shown. $^{***}P<0.001$.

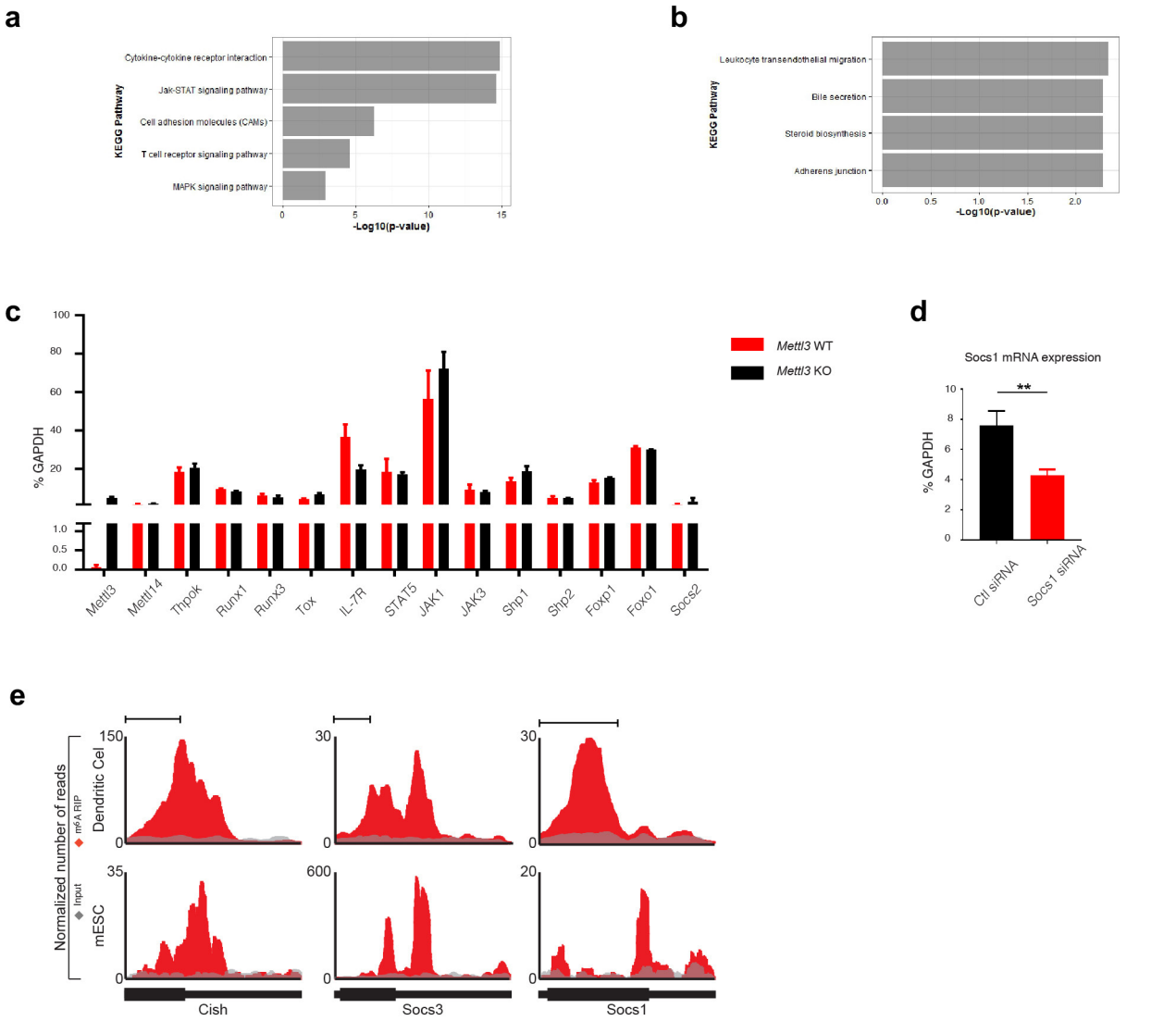

Extended Data Figure 5 | Socs genes are the m^{6}A targets that contribute to the observed phenotypes. a, Upregulated KEGG pathways in *Mettl3*-KO cells over wild-type cells based on RNA-seq data. **b**, Downregulated pathways in *Mettl3*-KO cells over wild-type cells. **c**, RT–qPCR validated the RNA-seq data, showing that the mRNA expression levels of other genes and regulators in IL-7 pathways did not change in *Mettl3*-KO naive T cells compared to wild-type cells ($n = 6$). **d**, *Socs1* siRNAs knock down *Socs1* gene expression by half *in vitro* ($n = 3$). Naive T cells were incubated with *Socs1* or control siRNA *in vitro* for 3 days, and RT–qPCR was used to measure the mRNA levels of *Socs1*. **e**, *Socs1*, *Socs3* and *Cish* mRNA 3′ UTRs are enriched with m^{6}A peaks from published ES cell and dendritic cell m^{6}A-RIP genome mapping. Red denotes the IP RNA counts, and grey denotes input. $n =$ number of biological replicates. Repeated three times and one set of data is shown. $^{**}P < 0.01$.

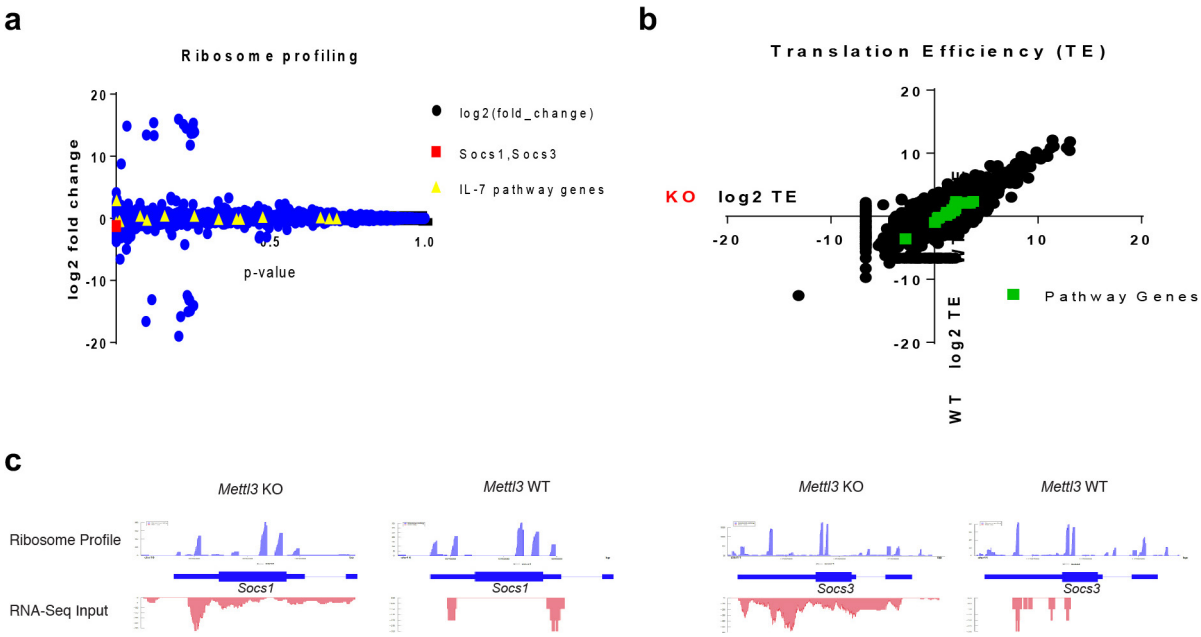

Extended Data Figure 6 | Ribosome profiling does not reveal any ribosome occupancy differences in IL-7 and TCR signalling related genes. a, Overall statistical analysis for all genes. Socs genes and other IL-7 pathway genes are highlighted. The *y*-axis is the $\log_2$ fold change of *Mettl3*-KO over wild type, and the *x*-axis plots the *P* value of the fold change value. **b**, Calculated translation efficiency for all genes, and the IL-7 and TCR pathway genes, do not show differences in translation efficiency between *Mettl3*-KO and wild-type naive T cells. **c**, Overall levels of RNA m^6A methylation in naive T cells from *Mettl3*-KO and wild-type mice. **c**, **d**, Example ribosome profiles of *Socs1* and *Socs3* mRNAs, which do not show any significant differences between wild-type (right panel) and *Mettl3*-KO (left panel) samples. The RNA-seq for the inputs are shown below the ribosome profiles, which also demonstrate enhanced mRNA expression for Socs genes.

a

	fast Deg	not fast Deg	
Up	21 *7.68* (23.10)	313 *326.32* (0.54)	334
not Up	112 *125.32* (1.42)	5338 *5324.68* (0.03)	5450
	133	5651	5784

$\chi^2 = 25.094$, df = 1, $\chi^2/df = 25.09$, $P(\chi^2 > 25.094) = 0.0000$

expected values are displayed in *italics*
individual χ^2values are displayed in (parentheses)

b

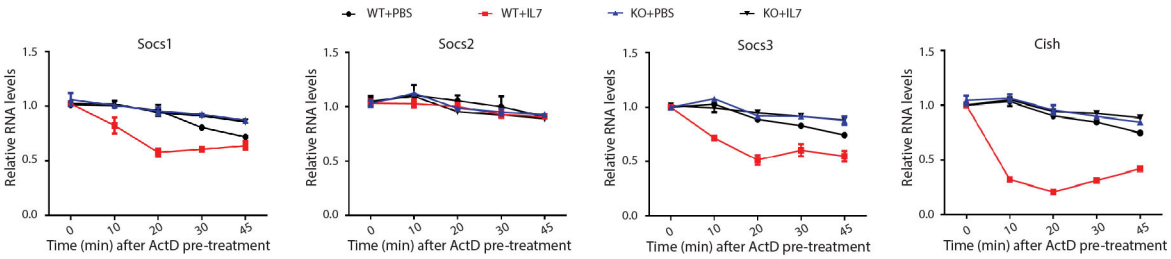

Extended Data Figure 7 | Socs genes are signal-inducible degradation-controlled genes. a, Upregulated genes in *Mettl3*-KO naive T cells are significantly enriched in the degradation-controlled group of genes from LPS-stimulated dendritic cells. We compared the genes that were differentially regulated by m^6A in naive T cells to degradation-controlled genes in dendritic cells. We can assign cluster information to 5,784 genes in our sequencing data set. We looked at the clusters where fast degradation played a key role (clusters 2, 4 and 6), and tested whether the number of genes upregulated was significant with a chi square test. The *P* value was <0.0001. 'Fast deg', genes in clusters 2,5,6; 'not fast deg', all other clusters; 'up', genes upregulated (marked as significant and positive fold change); 'not up', genes that did not change or were downregulated. **b**, *Socs1*, *Socs3* and *Cish*, but not *Socs2*, degraded faster upon IL-7 treatment in wild-type cells, and the faster degradation with IL-7 stimulation was abrogated in *Mettl3*-KO naive T cells. The naive T cells isolated from both wild-type and *Mettl3*-KO mice were pre-treated with actinomycin-D for 1 h to fully stop transcription before IL-7 stimulation, and the residual mRNAs at different time points were normalized back to $t = 0$ (100%).

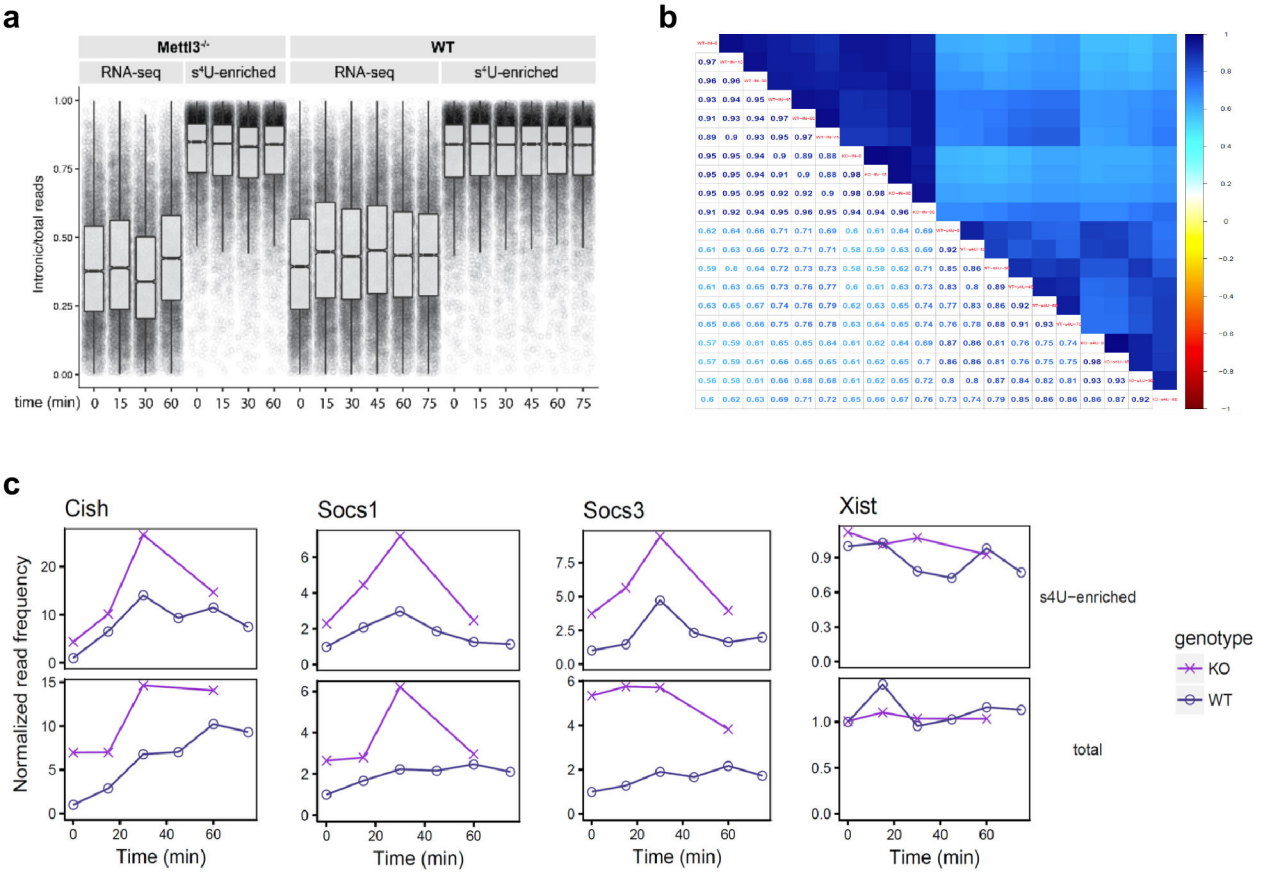

Extended Data Figure 8 | Summary of s^{4}U-seq data. a, Analysis of reads mapping to introns demonstrates high intronic read density in s^{4}U-enriched samples. The ratio of reads mapping to introns is expressed as a ratio to the total number of reads that map to each transcript in each sample. **b**, Plot illustrating the Spearman correlations of the transcript-level read frequencies in total and s^{4}U-enriched samples for wild-type and *Mettl3*-KO cells at various times after IL-7 stimulation. **c**, Changes in transcript frequencies after IL-7 stimulation for wild-type or *Mettl3*-KO cells with and without s^{4}U enrichment on the basis of s^{4}U-seq data. Expression levels are presented relative to the transcript levels of wild-type cells before IL-7 stimulation. Shown are cluster-3 *Socs* genes and a control gene *Xist*.

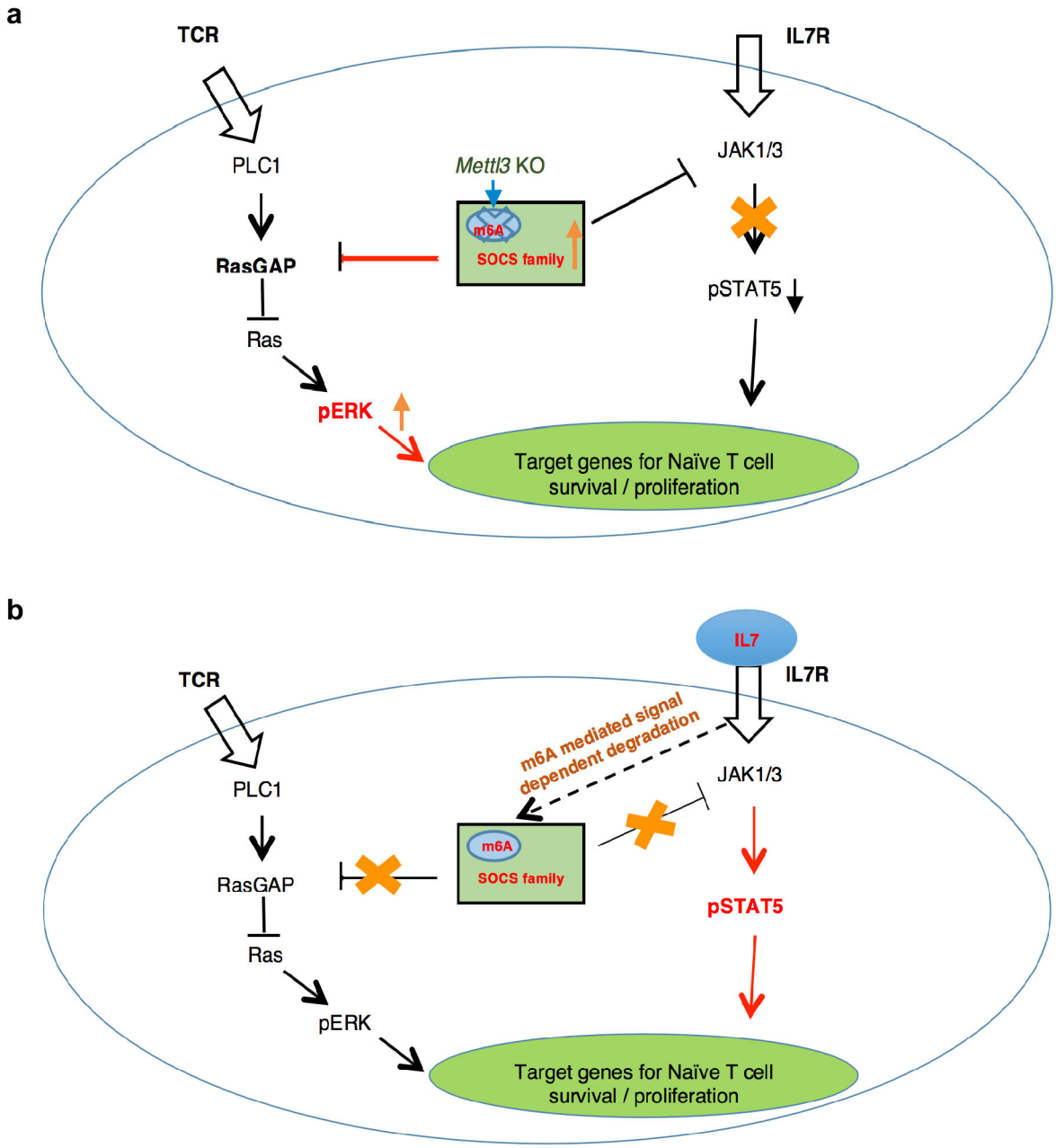

Extended Data Figure 9 | Working model for m^{6}A-controlled naive T cell homeostasis. a, *Mettl3*-KO naive T cell molecular mechanism: loss of m^{6}A leads to slower *Socs* mRNA degradation and increased SOCS protein levels, which blocks the IL7 pathway. **b**, Revised T cell differentiation model: m^{6}A targets *Socs1*, *Socs3* and *Cish* for inducible and rapid mRNA degradation upon IL-7 stimulation, allowing IL-7–JAKs signalling to activate the downstream target STAT5, to initiate the re-programming of the naive T cells for differentiation and proliferation.

nature research

Corresponding Author: Richard A. Flavell

Date: 6/1/2017

Life Sciences Reporting Summary

Nature Research wishes to improve the reproducibility of the work we publish. This form is published with all life science papers and is intended to promote consistency and transparency in reporting. All life sciences submissions use this form; while some list items might not apply to an individual manuscript, all fields must be completed for clarity.

For further information on the points included in this form, see Reporting Life Sciences Research. For further information on Nature Research policies, including our data availability policy, see Authors & Referees and the Editorial Policy Checklist.

Experimental design

1. Sample size

   Describe how sample size was determined.

   The sample size chosen for our animal experiments in this study was estimated based on our prior experience of performing similar sets of experiments.

2. Data exclusions

   Describe any data exclusions.

   No data were excluded from the analysis

3. Replication

   Describe whether the experimental findings were reliably reproduced.

   We at least independently repeated all the data once. All attempt to reproduce the results were successful.

4. Randomization

   Describe how samples/organisms/participants were allocated into experimental groups.

   All animal results were included and no method of randomization was applied.

5. Blinding

   Describe whether the investigators were blinded to group allocation during data collection and/or analysis.

   Binding is not relevant to our study, as we need to know the genotypes of the mouse strains.

   Note: all studies involving animals and/or human research participants must disclose whether blinding and randomization were used.

6. Statistical parameters

   For all figures and tables that use statistical methods, confirm that the following items are present in relevant figure legends (or the Methods section if additional space is needed).

n/a	Confirmed	
☐	☒	The exact sample size (*n*) for each experimental group/condition, given as a discrete number and unit of measurement (animals, litters, cultures, etc.)
☐	☒	A description of how samples were collected, noting whether measurements were taken from distinct samples or whether the same sample was measured repeatedly.
☐	☒	A statement indicating how many times each experiment was replicated
☐	☒	The statistical test(s) used and whether they are one- or two-sided (note: only common tests should be described solely by name; more complex techniques should be described in the Methods section)
☐	☒	A description of any assumptions or corrections, such as an adjustment for multiple comparisons
☐	☒	The test results (e.g. *p* values) given as exact values whenever possible and with confidence intervals noted
☐	☒	A summary of the descriptive statistics, including central tendency (e.g. median, mean) and variation (e.g. standard deviation, interquartile range)
☐	☒	Clearly defined error bars

See the web collection on statistics for biologists for further resources and guidance.

Software

Policy information about availability of computer code

7. Software

Describe the software used to analyze the data in this study.	RNA-seq was analyzed by Tophat & Cuffdiff & R package 'ggplot2'; Ribosome Profiling by tuxedo suit & R package; s4U Seq by STAR & HTSeq-count & R package INSPEcT/corrplot/maSigPro/pheatmap. All those information has been detailed in the method part.

For all studies, we encourage code deposition in a community repository (e.g. GitHub). Authors must make computer code available to editors and reviewers upon request. The *Nature Methods* guidance for providing algorithms and software for publication may be useful for any submission.

Materials and reagents

Policy information about availability of materials

8. Materials availability

Indicate whether there are restrictions on availability of unique materials or if these materials are only available for distribution by a for-profit company.	All mouse lines generated in the paper are freely available upon reasonable request. No other unique materials used.

9. Antibodies

Describe the antibodies used and how they were validated for use in the system under study (i.e. assay and species).	The detailed information on all antibodies were provided in the method section and extended data table 1. Those antibodies are all commercially available, and have been used routinely by other labs.

10. Eukaryotic cell lines

a. State the source of each eukaryotic cell line used.	No eukaryotic cell lines were used
b. Describe the method of cell line authentication used.	No eukaryotic cell lines were used
c. Report whether the cell lines were tested for mycoplasma contamination.	No eukaryotic cell lines were used
d. If any of the cell lines used in the paper are listed in the database of commonly misidentified cell lines maintained by ICLAC, provide a scientific rationale for their use.	No commonly misidentified cell lines were used

Animals and human research participants

Policy information about studies involving animals; when reporting animal research, follow the ARRIVE guidelines

11. Description of research animals

Provide details on animals and/or animal-derived materials used in the study.	We used both male and female C57BL/6 mice of all ages, we isolate T cells from mouse spleen and lympha nodes. The transgenic mouse lines we used include: Mettl3-f/f, Mettl14-f/f, CD4-Cre, RAG2-/-.

Policy information about studies involving human research participants

12. Description of human research participants

Describe the covariate-relevant population characteristics of the human research participants.	The research did not invovle human research participants.

nature research

Corresponding author(s): Richard A. Flavell

☐ Initial submission ☐ Revised version ☒ Final submission

Flow Cytometry Reporting Summary

Form fields will expand as needed. Please do not leave fields blank.

Data presentation

For all flow cytometry data, confirm that:

☒ 1. The axis labels state the marker and fluorochrome used (e.g. CD4-FITC).

☒ 2. The axis scales are clearly visible. Include numbers along axes only for bottom left plot of group (a 'group' is an analysis of identical markers).

☒ 3. All plots are contour plots with outliers or pseudocolor plots.

☒ 4. A numerical value for number of cells or percentage (with statistics) is provided.

Methodological details

5. Describe the sample preparation.	Cells from thymus, peripheral lymph nodes, mesenteric lymph nodes and spleen were isolated and used for FACS analysis. For sample preparation from spleen, erythrocytes were lysed and removed before FACS analysis.
6. Identify the instrument used for data collection.	The LSR II Flow Cytometer from BD Bioscience were used for FACS data collection.
7. Describe the software used to collect and analyze the flow cytometry data.	The FlowJo Software (Version 7.6.1) was used for FACS data analysis.
8. Describe the abundance of the relevant cell populations within post-sort fractions.	The purity of sorted cells was detected via flow cytometry immediately after sorting and samples with purity higher than 95% were used.
9. Describe the gating strategy used.	A FSC-H/FSC-A gate was used to determine single-cell populations. The boundaries between "positive" and "negative" were determined by the clear cell subpopulations and unstained negative controls.

Tick this box to confirm that a figure exemplifying the gating strategy is provided in the Supplementary Information. ☐